IEEE Access
Multidisciplinary | Rapid Review | Open Access Journal

Received July 16, 2021, accepted July 24, 2021, date of publication July 27, 2021, date of current version August 6, 2021.

*Digital Object Identifier 10.1109/ACCESS.2021.3100800*

# Frequency Regulation of Electric Vehicle-Penetrated Power System Using MPA-Tuned New Combined Fractional Order Controllers

**EMAD M. AHMED[1,2], (Senior Member, IEEE), AHMED ELMELEGI[2], AHMED SHAWKY[2], (Member, IEEE), MOKHTAR ALY[3], (Senior Member, IEEE), WALEED ALHOSAINI[1,4], (Member, IEEE), AND EMAD A. MOHAMED[2]**

[1]Department of Electrical Engineering, College of Engineering, Jouf University, Sakaka, Aljouf 72388, Saudi Arabia
[2]Department of Electrical Engineering, Faculty of Engineering, Aswan University, Aswan 81542, Egypt
[3]Facultad de Ingeniería y Tecnología, Universidad San Sebastián, Santiago 8420524, Chile
[4]Engineering and Applied Sciences Research Unit, Jouf University, Sakaka 72388, Saudi Arabia

Corresponding author: Mokhtar Aly (mokhtar.aly@uss.cl)

The authors extend their appreciation to the Deputyship for Research & Innovation, Ministry of Education in Saudi Arabia for funding this work through the project number ''375213500''. The authors also would like to extend their sincere appreciation to the central laboratory at Jouf University for support this study. This work is also supported in part by SERC Chile (ANID/FONDAP15110019) and by AC3E (ANID/Basal/FB0008).

**ABSTRACT** Energy transition from traditional generation sources into new renewable energy generation has become essential for facing climate changes. However, increased penetration levels of renewable energy sources (RESs) make power systems subjected to low inertia problems. Moreover, the continuously growing numbers of electric vehicles (EVs) have made the substantial need for their contribution in power systems. Therefore, this paper proposes a combined fractional-order controller using the parallel combination of tilt-integral-derivative with filter (TIDF) and hybrid fractional-order (HybFO) controllers for robust frequency regulation in interconnected power systems. The proposed controller is advantageous in combining the merits of two fractional-order controllers that result in more robust and effective load frequency control (LFC) at wide range and different types of disturbances. Furthermore, a new application of marine predator optimization algorithm (MPA) is proposed for simultaneously determining the optimum controller parameters in the different power system areas. The existing EVs contribute in performing additional functionality in power systems. EVs help in damping out the frequency and tie-line power oscillations in the proposed work. The two-area interconnected power system is selected as a case study with the installed photovoltaic (PV), and wind generations in addition to distributed EVs among areas. The obtained results show the superiority and suitability of the proposed controller over the traditional controllers in the literature. Additionally, the effectiveness of the MPA is validated and compared with recent meta-heuristic optimization algorithms.

**INDEX TERMS** Electric vehicles (EVs), interconnected power systems, load frequency control (LFC), marine predator optimization algorithm (MPA), renewable energy sources (RESs).

## I. INTRODUCTION

### A. GENERAL

Climate changes have driven governments to set ambitious plans for renewable energy sources (RESs) replacement of conventional fossil fuel sources [1]. Vast installations of wind and photovoltaic (PV) generation systems have been deployed in operation in recent years [2]. However, RESs possess low inertial response due to their power electronics based structures. Due to the intermittent nature of RESs, power systems are subjected to frequency oscillations, which can lead to severe consequences, such as partial/complete power system blackout. Moreover, changes in the demanded load and resulting power mismatches between generation and loading lead to frequency deviations and tie-line power fluctuation from their nominal values. Therefore, load frequency

The associate editor coordinating the review of this manuscript and approving it for publication was Chandan Kumar.

control (LFC) has become a crucial element for preserving stable and secure power system operation [3].

The LFC performs an important role in maintaining the stability of the interconnected power system during load disturbances and RESs variations. In general, frequency regulation in power systems includes two different control loops. The first loop is represented by the primary control loop, which deals with the speed governor regulation. However, the primary control loop is not sufficient for controlling and overcoming the power system fluctuations. The second loop is based on the secondary control loop, which contributes mainly in handling frequency variations and the fluctuations in tie-line power among the different system areas [4], [5]. Different energy storage devices (ESDs) can participate in improving power systems performance. In addition, ESDs can help in maintaining the stability and durability of the system frequency during the various fluctuations. An overall increase of running electric vehicles (EVs) has been achieved in recent years, and further exponential growth is also expected in the near future. Accordingly, adding more features for EVs in contributing and enhancing the power system response is essential with the continuously increased numbers of EVs. The storage devices of EVs are utilized as distributed ESDs in power systems. As a result, more robust and stable controllers are needed for preserving high power quality and secure energy supply of the power systems [6].

### B. LITERATURE REVIEW

Through the increased and board utilization of EVs, the role of their energy storage systems in enhancing LFC and power system stability cannot be neglected. The fleets of EVs can be considered as distributed energy storage devices that can be congregated to discharge during the load demand. However, in large power systems consisting of many interconnected areas, there are many control parameters, which need to be optimally designed. In the literature, there are several optimized controllers based on integer-order, fractional-order (FO), fuzzy logic (FL), artificial intelligence (AI) control systems [7]–[9]. Different arrangements and combinations using proportional (P), integral (I), derivative (D), and tilt (T) controllers have been proposed for LFC systems [10], [11]. Table. 1 summarizes the used abbreviations in this paper. The conventional PI controller has been developed for LFC in [12]. However, it suffers from instability issues when communication system time delay is considered.

Using different control theories, the parameters of LFC in interconnected power systems have been designed. In [13], PID controller parameters have been designed based on stability boundary locus (SBL) scheme. In [14], PI parameters are optimized using Harris Hawks optimization (HHO). These controllers represent simple solutions, however, they fail at totally mitigating the fluctuations in power systems. The control of EVs using TID controller has been designed and optimized using artificial-bee-colony optimizer (ABC) in [15]. Also, in [16], the authors have presented optimum modified FO controller for EVs based on two-area interconnected power systems. Furthermore, virtual inertial controllers have been optimized using the particle swarm optimizer (PSO) algorithm [17]. Moreover, an improved automatic generation control (AGC) method using FFOID has been developed in [18]. TID controller has been implemented for LFC and optimized using pathfinder algorithm (PFA) [19]. In [20], a FO-PID controller has been optimally designed based on a movable damped wave algorithm (MDWA) in multi-area power system. In [21], FOPID controller has been proposed based on sine-cosine optimization algorithm (SCA). However, these control techniques cannot damp out wide range of fluctuations due to using single degree of freedom.

Moreover, in [6], [22]–[24], the various FO-based controllers have been presented and compared for solving LFC issues. The comparison included the PID, FOPID, two-degree-of-freedom (2DOF)-PID, 2DOF-FOPID, 3DOF-PID, 3DOF-FOPID, and CF-FOIDF. However, most of the addressed controllers require massive efforts in the tuning process of the parameters. Particularly, the metaheuristic optimization techniques lack the reliability due to the increased probability to settle in a local minimum. In addition, several parameters need to be tuned properly, which represents a big issue to provide the optimal solution.

In order to obtain further improvements of the LFC performance, modified control structures have been introduced in the literature. The TIDF controller has been proposed and optimized using differential evolution optimization (DE) in [25]. PI-TDF controller has been tuned using slap swarm optimizer algorithm (SSA) in [26]. Dual stage controllers have been optimized using butterfly optimizer algorithm (BOA) in [27]. Manta ray foraging optimizer is used for designing hybrid FO controllers in [28]. Furthermore, cascaded FOPID-FLC have been designed for damping power system oscillations using imperialist competitive optimizer algorithm (ICA) in [29]. While, in [30], an improved FPIDN-FOPIDN control scheme has been developed for AGC using ICA in two-area power systems. In [31], an adaptive integrator has been introduced using elder scrolls online (ESO) and balloon effect modulation (BE). Merging ESO with BE is beneficial in improving system stability especially with parameters uncertainties. Moreover, a new AGC controller using cascaded FO-ID with filter has been presented in [32].

The optimized modern controllers have been applied in LFC of interconnected power systems. Model predictive control (MPC) has been optimized using sooty terns optimizer (STO) in [33], [34] and multi-verse optimization (MVO) in [35]. As well, sliding mode control (SMC) has been designed and optimized using ABC in [36], [37]. However, developing MPC and SMC requires more complex and accurate mathematical models for the power system. Moreover, FLC systems have been presented for controlling EVs in interconnected power system using ICA, genetic algorithm and tribe DE optimizer in [38], [39]. The classification of the various addressed LFC techniques in the literature has been

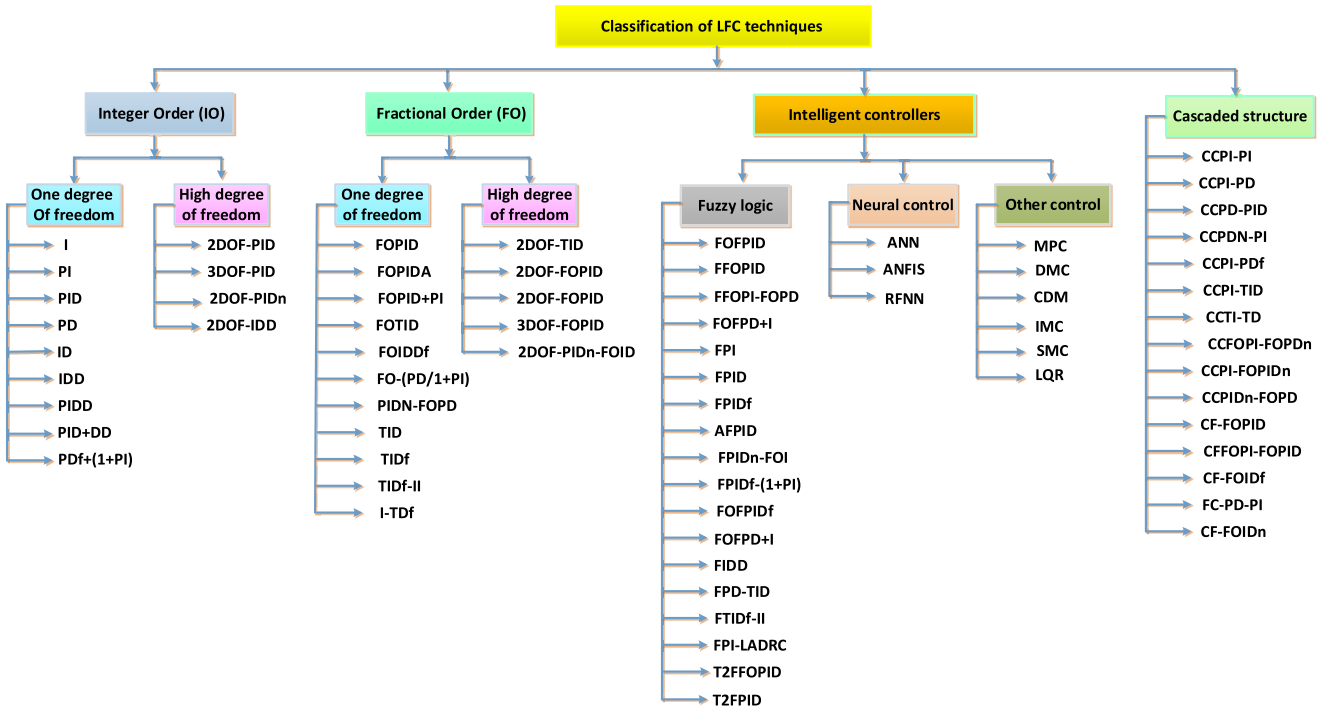


**FIGURE 1.** Classification of different LFC techniques.

shown in Fig. 1. The meaning of the different abbreviations are clarified in Table. 1.

**TABLE 1.** Abbreviations of various control techniques in this paper.

| Symbol | Meaning |
|---|---|
| I | Integral |
| P | Proportional |
| D | Derivative |
| 2DOF | Two degree of freedom |
| 3DOF | Three degree of freedom |
| FO | Fractional order |
| A | Accelerated |
| n,f | Filter |
| F | Fuzzy |
| T | Tilt |
| ANN | Artificial neural network |
| ANFIS | Adaptive neuro-fuzzy inference system |
| RFNN | Random fuzzy neural network |
| DMC | Dual mode control |
| CDM | Coefficient diagram method |
| IMC | Internal model control |
| LQR | Linear quadratic regulator |
| CC | Cascaded |

### C. ARTICLE MOTIVATION

From the aforementioned discussion, many controllers have been presented in the area of LFC in interconnected power systems. However, using FO-based controllers has excellent advantages in damping system oscillations and regulating system frequency. Moreover, they provide practical and robust solutions regarding response time and frequency regulations. Therefore, this paper proposes a combined FO controller using the parallel combination of TIDF and HybFO controllers for robust frequency regulations in interconnected power systems. The proposed controller is advantageous in combining the merits of two FO controllers that result in more robust and effective frequency regulation with wide range and different types of disturbances. The proposed parallel combination employs two feedback signals using the frequency deviation and the area control error (ACE). This, in turn, leads to damping the high-frequency oscillations using the frequency deviation loop. In addition, damping the low-frequency oscillations is achieved through the ACE loop.

Moreover, thanks to the authors' knowledge, a new application of MPA is proposed for simultaneously determining the optimum controller parameters. The advantageous capabilities of MPA result from its operating principle through emulating the food search process within the surrounding predators by the movements of Levy and Brownie. The MPA can optimally encounter modified policy through the biological interactions between the preys and predators. The MPA takes the benefits of the good memory within reminding their associates and locations of successful foraging [40]–[43].

### D. ARTICLE CONTRIBUTIONS

The main contributions of this paper can be summarized in the following points:

- A new robust fractional order controller is proposed based on the combination of TIDF and HybFO controllers for frequency stability improvement of power system. The proposed controller can quickly damp out the frequency oscillations and tie-line power deviations.
- The proposed controller incorporates the features of the optimal centralized combination of the TIDF and

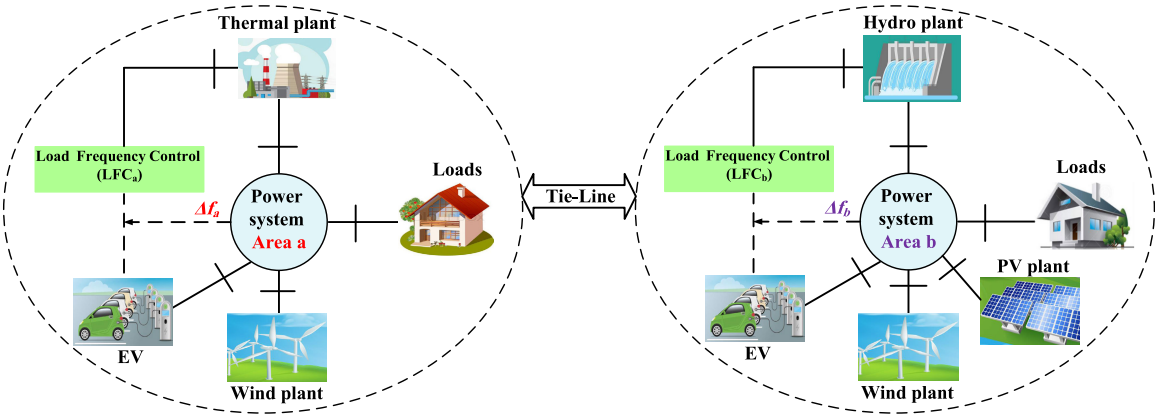


**FIGURE 2.** The main structure and components of the two-area interconnected power systems.

HybFO controllers for enhancing the response of the whole LFC system.

- This study proposes the contribution of EVs in providing an adequate inertia power to the power system during contingencies. Thus, EVs can participate in achieving more damping of the frequency and tie-line power oscillations.
- A new application of the MPA is developed for optimizing the parameters of the proposed controller. The superiority of the MPA is employed for optimally determining the parameters of the proposed controller.
- The proposed controller is applied with considering the different effects of load changes and unpredictable disturbances of RESs penetration levels in addition to their uncertainties. Furthermore, the generation rate constraints (GRC) are considered in the design process of the proposed controller.
- The performance of the proposed TIDF/HybFO combined controller based on the MPA is compared with the conventional TIDF and HybFO controllers. The proposed controller can significantly guarantee reliable performance of the interconnected power system and improved frequency stability with considering the high deployment of RESs.

The remaining of the paper is organized as follows: Section II provides the mathematical model of the interconnected power system, including the various generation sources. The proposed HybFO-TIDF controller is presented in Section III. Section IV provides the details of the MPA and the proposed design optimization process. Section V presents the simulation results and discussions of the proposed controller. The performance comparisons are presented in Section VI. Finally, paper conclusion is provided in Section VII.

## II. MATHEMATICAL MODELLING OF THE STUDIED SYSTEM

### A. STRUCTURE OF STUDIED POWER SYSTEM

In the current work, the studied power system consists of two interconnected areas through AC tie-line, as shown in Fig. 2. Area *a* contains non-reheat thermal power plant, wind turbine, EVs and connected loads. Whereas, area *b* includes a hydro power plant, PV power plant, wind power plant, the connected EVs, and loads as shown in Fig. 3. In addition, each area is controlled by its local LFC to minimize the fluctuations in area frequency and tie-line power. The tuning process of these controllers is crucial for determining the performance of each area with the various transients in the system. This paper proposes a new controller and optimized design algorithm for LFC in the studied two-area power system. In the studied system, the proposed controller also manages the connected EVs in each area for preserving robust control of the system frequency and tie-line power. Furthermore, the proposed system employs the expected future EVs in power systems to enhance system performance and response. Therefore, more stable power system operation is obtained against the various operating conditions, such as step changes in the power system loading, the resulting low inertia effects due to high penetrations levels of RESs, and the uncertainties in the system parameters. The values of basic simulation parameters of studied systems are tabulated in Table. 2 as given in [28]. In the following subsections, the mathematical modeling of the various elements is introduced.

### B. EV MODELLING

Recently, with the wide replacements of traditional fossil fuel-based vehicles by EVs, additional functions are added to control the EVs to improve the response of power systems, efficiency, and reliability. One main task is maintaining the power system frequency stability caused by step changes and variations of generated power from RES and absorbed power by connected loads. The detailed dynamic model of EVs is shown in Fig. 4, which has been applied in this paper for the frequency response analysis as in [16]. In addition, the Nernst equation is commonly utilized for expressing the relation among the open circuit voltage ($V_{oc}$) and the state of charge (SOC) of connected EVs as follows [16]:

$$V_{oc}(SOC) = V_{nom} + S\,\frac{RT}{F} ln\,(\frac{SOC}{C_{nom} - SOC}) \qquad (1)$$

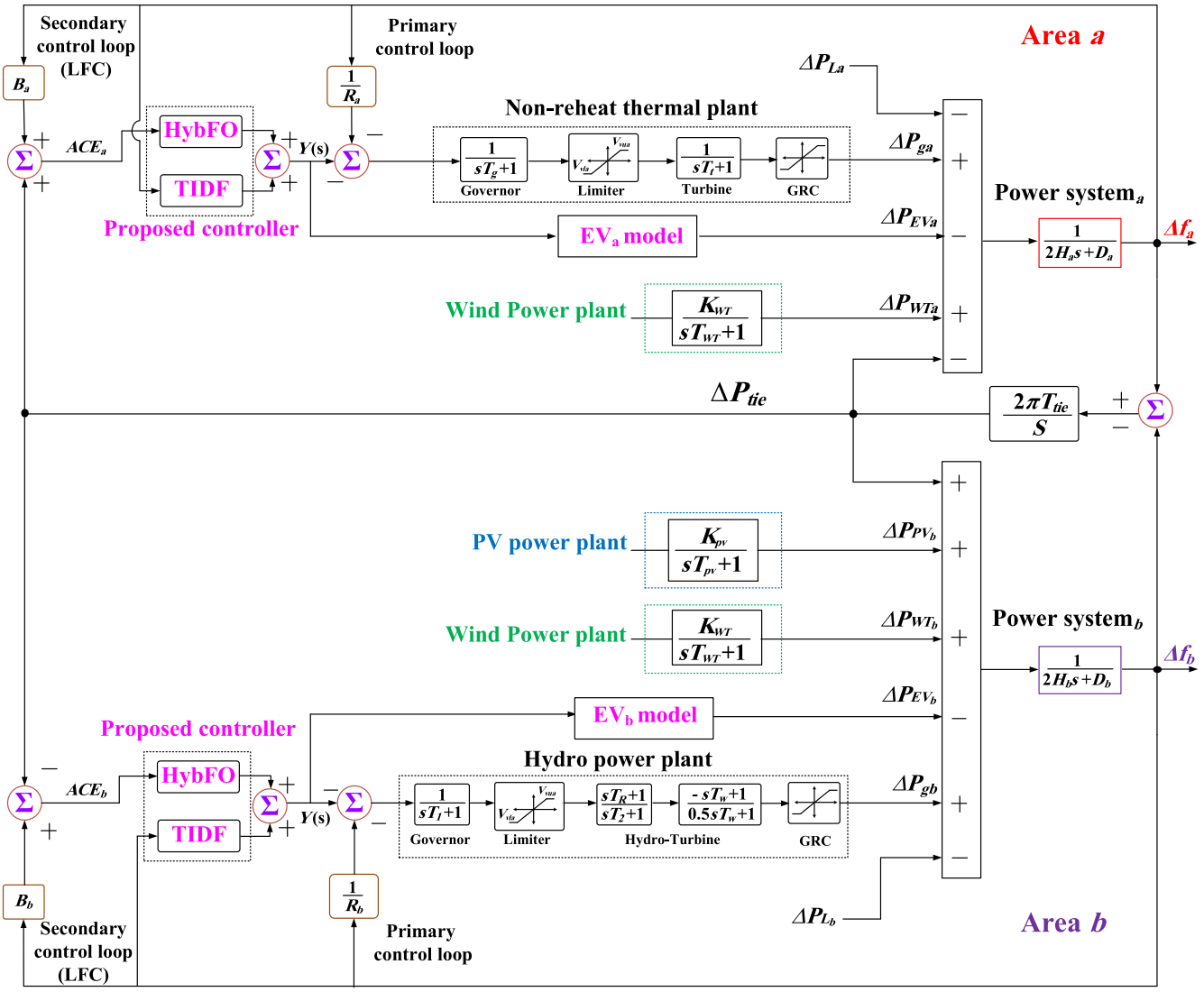


**FIGURE 3.** The model of studied system using two-area interconnected power systems.

where $V_{oc}(SOC)$, $V_{nom}$, $C_{nom}$ are the EVs open-circuit voltages as a function of EVs $SOC$, EVs nominal voltages and EVs nominal capacities (in Ah), respectively. In addition, $S$ denotes to sensitivity parameter value between $V_{oc}$ and the $SOC$ of connected EVs. Whereas, $R$, $F$, $T$ represent the gas constant, Faraday constant, and the temperature, respectively.

### C. MODELLING OF WIND POWER PLANTS

In this work, simplified modeling of wind power plants is employed to emulate the variable nature of the generated output power from wind generation system. The employed first-order transfer function $G_{WT}(s)$ of wind power plants can be expressed as follows [17]:

$$G_{WT}(s) = \frac{K_{WT}}{T_{WT}s + 1} \tag{2}$$

where, $K_{WT}$ and $T_{WT}$ represent the gain and time constant for the wind power plant, respectively.

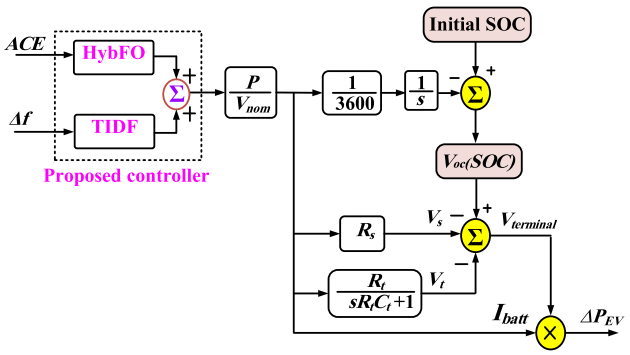


**FIGURE 4.** Dynamic modeling of connected EVs for LFC studies.

### D. MODELLING OF PV POWER PLANTS

In the same context, the transfer function of PV power plants $G_{PV}(s)$ is modeled through a first-order transfer function

**TABLE 2.** Main values of simulation system data with ($i \in \{a, b\}$).

| Data | Abbreviations | Values | |
|---|---|---|---|
| | | Area $a$ | Area $b$ |
| **LFC model** | | | |
| Droop constant | $R_i$ (Hz/MW) | 2.4 | 2.4 |
| Frequency bias | $B_i$ (MW/Hz) | 0.4249 | 0.4249 |
| **Power system** | | | |
| Capacity of area | $P_{ri}$ (MW) | 1200 | 1200 |
| inertia constants | $H_i$ (p.u.s) | 0.0833 | 0.0833 |
| damping coefficients | $D_i$ (p.u./Hz) | 0.00833 | 0.00833 |
| Capacity ratio gain | $A_{ab}$ | -1 | |
| Tie-line coefficient | $T_{tie}$ (s) | 0.0865 | |
| **Non-Reheat thermal plant** | | | |
| Min. limit of valve gate | $V_{vli}$ (p.u.MW) | -0.5 | -0.5 |
| Max. limit of valve gate | $V_{vui}$ (p.u.MW) | 0.5 | 0.5 |
| TC of the thermal governor | $T_g$ (s) | 0.08 | - |
| TC of the thermal turbine | $T_t$ (s) | 0.3 | - |
| **Hydro power plant** | | | |
| Min. limit of valve gate | $V_{vli}$ (p.u.MW) | -0.5 | -0.5 |
| Max. limit of valve gate | $V_{vui}$ (p.u.MW) | 0.5 | 0.5 |
| TC of governors | $T_1$ (s) | - | 41.6 |
| TC of transient droops | $T_2$ (s) | - | 0.513 |
| Governor reset time | $T_R$ (s) | - | 5 |
| Water starting time | $T_w$ (s) | - | 1 |
| **PV power plant** | | | |
| TC for PV | $T_{PV}$ (s) | - | 1.3 |
| PV gain | $K_{PV}$ (s) | - | 1 |
| **Wind power plant** | | | |
| TC for Wind | $T_{WT}$ (s) | 1.5 | 1.5 |
| Wind gain | $K_{WT}$ (s) | 1 | 1 |
| **EV model** | | | |
| Penetration levels | - | 5-10% | 5-10% |
| Nominal voltages | $V_{nom}$ (V) | 364.8 | 364.8 |
| Nominal battery capacities | $C_{nom}$ (Ah) | 66.2 | 66.2 |
| Series resistances | $R_s$ (ohms) | 0.074 | 0.074 |
| Transient resistances | $R_t$ (ohms) | 0.047 | 0.047 |
| Transient capacitances | $C_t$ (farad) | 703.6 | 703.6 |
| Constant value | $RT/F$ | 0.02612 | 0.02612 |
| Maximum limit SOC of Battery | % | 95 | 95 |
| Battery energy capacity | $C_{batt}$(kWh) | 24.15 | 24.15 |

* TC represent time constant

model. It can be expressed as follows [18]:

$$G_{PV}(s) = \frac{K_{PV}}{T_{PV}s + 1} \tag{3}$$

where, $K_{PV}$ and $T_{PV}$ denote to the gain and time constant for the employed PV power plants, respectively.

### E. MODELLING OF NON-REHEAT THERMAL POWER PLANTS

As shown in Fig. 3, the modeling of non-reheat thermal power plants is composed of the governor stage, limiter stage, turbine stage, and generation rate constraint (GRC) stage [20]. The governor stage can be expressed as follows:

$$G_g(s) = \frac{1}{T_g s + 1} \tag{4}$$

whereas, the turbine stage can be expressed as following:

$$G_t(s) = \frac{1}{T_t s + 1} \tag{5}$$

The definitions of the various elements and their corresponding values for the current study are detailed in Table. 2.

## III. PROPOSED HybFO-TIDF CONTROLLER

In literature, various integer and fractional order controllers are utilized for LFC in several power systems applications. The PID has found wide employments in frequency stability problems in the literature. The transfer function of the PID controller is expressed as follows:

$$C(s) = \frac{Y(s)}{R(s)} = K_p + \frac{K_i}{s} + K_d\ s \tag{6}$$

where, $K_i$, $K_p$, and $K_d$ represent the gains for the integral, proportional, and derivative terms, respectively. The fractional order (FO) PID controller has been also introduced for combining the merits of integer order PID and the FO calculus. The FOPID controller can be represented by the following transfer function:

$$C(s) = \frac{Y(s)}{R(s)} = K_p + \frac{K_i}{s^{\lambda}} + K_d\ s^{\mu} \tag{7}$$

where, $\lambda$ and $\mu$ denote to the orders for the integral, and derivative terms, respectively. Their tuning range lies in the limits between [0, 1]. It has been verified in literature that adding the FO terms $\lambda$ and $\mu$ can provide better performance and enhanced dynamic responses compared to the PID controllers [28].

From another side, tilt integral derivative (TID) controllers have been proposed in the literature for extending the applications of FO control systems in LFC. The TID controller can be expressed by the following transfer function:

$$C(s) = \frac{Y(s)}{R(s)} = K_t\ s^{-(\frac{1}{n})} + \frac{K_i}{s} + K_d\ s \tag{8}$$

where, $K_t$, $K_i$, $K_d$ represents the gains of tilt, integral, and derivative terms. The tuning process of the gain terms and FO terms gains are employed for optimizing and providing robust performance in the overall power system. Whereas, $n$ represents a non-zero real number, and it is selected in the range between 2.0 and 5.0 [11], [25].

The HybFO controller has been presented in [28] by combining the characteristics of both the TID and FOPID controllers. The presented controller has proven superior performance over the traditional PID, TIDF, and HybFO controllers. The transfer function of the HybFO controller can be represented as follows:

$$C(s) = \frac{Y(s)}{R(s)} = K_t\ s^{-(\frac{1}{n})} + \frac{K_i}{s^{\lambda}} + K_d\ s^{\mu} \tag{9}$$

From the aforementioned existing controllers in literature, new developments are needed for widening the applications of FO control systems. The traditional controllers employs a single feedback signal (ACE signal), which results in slow response of the LFC system. In addition, improper mitigation of various disturbances is obtained through using only the ACE feedback signal. From another side, the proposed controller in this paper is based on combining the merits of both HybFO and TIDF controllers. The proposed controller combines the superior performance of the HybFO and TIDF controllers over the traditional controllers. The

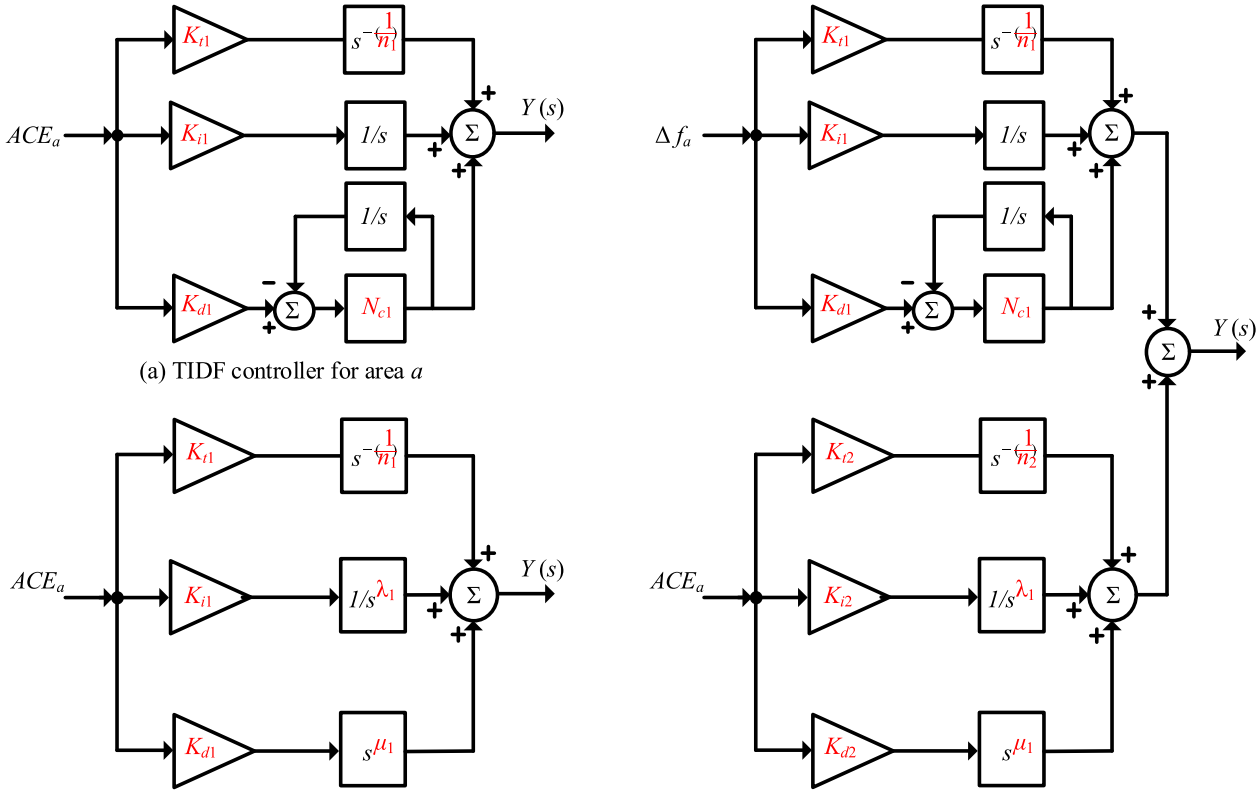


(a) TIDF controller for area $a$

(b) HybFO controller for area $a$

(c) The propsoed HybFO-TIDF controller for area $a$

**FIGURE 5.** The derivation of the structure of the proposed controller.

proposed controller combines two different inputs, including the frequency deviations in each area, and the ACE signal of the area. The employment of the two feedback signals in the proposed controller is advantageous at damping both of the high-frequency and low-frequency oscillations. The frequency deviation loop can mitigate the high-frequency system fluctuations. Whereas, the ACE control loop can mitigate the low frequency fluctuations. Therefore, improved system response is guaranteed through applying the proposed controller.

In the proposed controller, the frequency deviation loop is based on the TIDF controller, whereas the HybFO controller is utilized in the ACE loop. The mathematical representation of the proposed controller can be expressed as follows:

$$Y(s) = (K_{t1}\, s^{-(\frac{1}{n_1})} + \frac{K_{i1}}{s} + K_{d1}\, \frac{N_c s}{s + N_c})\Delta f_x + (K_{t2}\, s^{-(\frac{1}{n_2})} + \frac{K_{i2}}{s^{\lambda_1}} + K_{d2}\, s^{\mu_1})ACE_x \quad (10)$$

where, $N_c$ represents the derivative filter coefficient of the TIDF controller, and ($x \in \{a, b\}$). Fig. 5 shows the structure of the HybFO, TIDF, and the proposed controller for area $a$. In the following section, the design process using the proposed optimization procedures will be introduced. The tuning of various parameters of LFC is optimally determined.

In this paper, the widely-used Oustaloup method is employed for representing various fraction order control methods [28]. The approximate model of the operator transfer function possesses $(2M + 1)$ number of poles/zeros, in which $M$ is selected to be five. The frequency range for the representation of fractional order system is selected in the range $[-1000, 1000]$ rad/s.

## IV. THE PROPOSED OPTIMIZED DESIGN PROCESS

### A. THE MPA OPTIMIZER

The proposed design process is based on using the recently developed MPA optimizer. The MPA is utilized for determining optimally the various parameters of the proposed HybFO-TIDF controller. The main operating principle of MPA is based on searching process of the food strategy represented by movement of the Levy and Brownie within surrounding predators in addition to optimal encounters of modified policies within biological interactions among preys and predators. The reminding is their associates in addition to locations of the successful foraging. The MPA procedures are composed of three different phases according to the ratio of speed between the preys and predators. In the following, the explanations and simplified mathematical modelling of the MPA are introduced.

#### 1) PHASE NO. 1 AT HIGH RATIO OF SPEED

The speed of preys is assumed to be higher than the speed of predators. This stage is represented with the first one-third of the iterations. In which, the preys follow subsequent relations for modifying their locations. This stage is represented as follows:

$$S_{\mathrm{i}} = R_{\mathrm{B}} \times (Elite_{\mathrm{i}} - R_{\mathrm{B}} \times Z_{\mathrm{i}}), \quad i = 1, 2, \ldots, n \tag{11}$$

$$Z_{\mathrm{i}} = Z_{\mathrm{i}} + P.R \times S_{\mathrm{i}} \tag{12}$$

where, $R \in [0, 1]$ represent a random numbers vector, $P = 0.5$, and $R_B$ represents the vector of Brownian motion.

#### 2) PHASE NO. 2 AT UNITY RATIO OF SPEED

In this stage, the speed of preys equals to the speed of predators. This stage is represented with the second one-third of the iterations. In this stage, the Brownian and Lévy flight approaches represent the movements types of predators and preys, respectively. The population in this stage is represented by two subsections, wherein first subsection uses (13), and (14). Whereas, (15) and (16) are used in the second subsection for modifying the locations as following: detailed operation and principles of the MPA with mathematical models have been introduced in [44].

$$S_{\mathrm{i}} = R_{\mathrm{L}} \times (Elite_{\mathrm{i}} - R_{\mathrm{L}} \times Z_{\mathrm{i}}), \quad i = 1, 2, \ldots, n/2 \tag{13}$$

$$Z_{\mathrm{i}} = Z_{\mathrm{i}} + P.R \times S_{\mathrm{i}} \tag{14}$$

where, $R_L$ represents a randomly generated variable through Lévy distribution.

$$S_{\mathrm{i}} = R_{\mathrm{B}} \times (R_{\mathrm{B}} \times Elite_{\mathrm{i}} - Z_{\mathrm{i}}), \quad i = 1, 2, \ldots, n/2 \tag{15}$$

$$Z_{\mathrm{i}} = Elite_{\mathrm{i}} + P.CF \times S_{\mathrm{i}} \tag{16}$$

where,

$$CF = (1 - \frac{t}{t_{\max}})^{2\frac{t}{t_{\max}}} \tag{17}$$

where, $t$ and $t_{\max}$ represent the current and the maximum iterations numbers.

#### 3) PHASE NO. 3 AT LOW RATIO OF SPEED

In this stage, the speed of predators is larger than the speed of preys in contrary to stage No.1. This stage is represented in the last one-third of the iterations. In which, the modification of locations is made using the following model:

$$S_{\mathrm{i}} = R_{\mathrm{L}} \times (R_{\mathrm{L}} \times Elite_{\mathrm{i}} - Z_{\mathrm{i}}), \quad i = 1, 2, \ldots, n \tag{18}$$

$$Z_{\mathrm{i}} = Elite_{\mathrm{i}} + P.CF \times S_{\mathrm{i}}, \quad CF = (1 - \frac{t}{t_{\max}})^{2\frac{t}{t_{\max}}} \tag{19}$$

### B. OBJECTIVE FUNCTION AND OPTIMIZATION PROCESS

The MPA is employed for the determination of optimal parameters in the proposed controller. There are 11 parameters in each area, which have to be simultaneously determined. The parameters of each area include the following parameters ($K_{t1}$, $K_{t2}$, $K_{i1}$, $K_{i2}$, $K_{d1}$, $K_{d2}$, $n_1$, $n_2$, $\lambda_1$, $\mu_1$, and $N_{c1}$ in area $a$) and ($K_{t3}$, $K_{t4}$, $K_{i3}$, $K_{i4}$, $K_{d3}$, $K_{d4}$, $n_3$, $n_4$, $\lambda_2$, $\mu_2$, and $N_{c2}$ in area $b$). Therefore, total of 22 parameters are required to be determined simultaneously for preserving optimized determination of the values.

The objective function for the optimization process has to maintain minimized values for the frequency deviations in each area ($(\Delta f_a)$ of area $a$ and $(\Delta f_b)$ in area $b$ in addition to minimized values of the tie-line power ($\Delta P_{tie}$). The four widely-used error estimation methods are used in the proposed optimization process, including the integral-squared error (ISE), the integral time-squared error (ITSE), the integral absolute error (IAE) and Integral time absolute error (ITAE). The four methods are used to verify the effectiveness and superiority of proposed controller and optimizer based on the desired limitations and specifications. They are represented as follows:

$$ISE = \int_0^{t_s} ((\Delta f_a)^2 + (\Delta f_b)^2 + (\Delta P_{tie})^2)\, \mathrm{d}t \tag{20}$$

$$IAE = \int_0^{t_s} (abs(\Delta f_a) + abs(\Delta f_b) + abs(\Delta P_{tie}))\, \mathrm{d}t \tag{21}$$

$$ITSE = \int_0^{t_s} ((\Delta f_a)^2 + (\Delta f_b)^2 + (\Delta P_{tie})^2)\, t.\mathrm{d}t \tag{22}$$

$$ITAE = \int_0^{t_s} (abs(\Delta f_a) + abs(\Delta f_b) + abs(\Delta P_{tie}))\, t.\mathrm{d}t \tag{23}$$

The MPA determines the optimum parameters within the predefined upper and lower limits of each parameter. The selected limits for the proposed optimization process are as follows:

$$\begin{aligned}
K_t^{min} &\le K_{t1}, K_{t2}, K_{t3}, K_{t4} \le K_t^{max} \\
K_i^{min} &\le K_{i1}, K_{i2}, K_{i3}, K_{i4} \le K_i^{max} \\
K_d^{min} &\le K_{d1}, K_{d2}, K_{d3}, K_{d4} \le K_d^{max} \\
n^{min} &\le n_1, n_2, n_3, n_4 \le n^{max} \\
\lambda^{min} &\le \lambda_1, \lambda_2 \le \lambda^{max} \\
\mu^{min} &\le \mu_1, \mu_2 \le \mu^{max} \\
N_c^{min} &\le N_{c1}, N_{c2} \le N_c^{max}
\end{aligned} \tag{24}$$

where, $(f)^{min}$ and $(f)^{max}$ represent the minimum and the maximum limit values of each parameter in proposed HybFO-TIDF controller. In the proposed design approach, $K_t^{min}$, $K_i^{min}$, and $K_d^{min}$ are set to 0, whereas, $K_t^{max}$, $K_i^{max}$, and $K_d^{max}$ are set to 5. The values of $n^{min}$ and $n^{max}$ are selected as 2 and 5, respectively. The values of $\lambda^{min}$, and $\mu^{min}$ are set to 0, whereas, $\lambda^{max}$, and $\mu^{max}$ are selected to be 1. Additionally, the parameter $N_c^{min}$, and $N_c^{max}$ are selected to be 5 and 500, respectively. Table 3 summarizes the all optimized values of controllers parameters.

## V. SIMULATION RESULTS AND DISCUSSIONS

The performance of the proposed controller and the operation of the MPA are studied and evaluated using the selected

**TABLE 3.** Obtained optimum values of the studied controller parameters for each area based on Fig. 5.

| Controller | Area | Control | Coefficients | | | | | | | | | | |
|---|---|---|---|---|---|---|---|---|---|---|---|---|---|
| | | | $K_{t1}$ | $K_{i1}$ | $K_{d1}$ | $K_{t2}$ | $K_{i2}$ | $K_{d2}$ | $n_1$ | $Nc_1$ | $n_2$ | $\lambda_1$ | $\mu_1$ |
| Proposed | Area $a$ | LFC | 1.8563 | 1.993 | 1.9104 | 1.8656 | 1.8299 | 1.8308 | 4.3174 | 55.9104 | 3.0794 | 0.92591 | 0.54107 |
| | Area $b$ | LFC | 1.079 | 0.84591 | 1.9164 | 1.4216 | 0.73848 | 1.8472 | 3.8943 | 166.9571 | 3.7763 | 0.9139 | 0.50954 |
| HybFO | Area $a$ | LFC | 1.981 | 1.9487 | 1.8505 | - | - | - | 4.5971 | - | - | 0.86854 | 0.46745 |
| | Area $b$ | LFC | 1.7034 | 1.4318 | 0.32546 | - | - | - | 4.722 | - | - | 0.43551 | 0.55539 |
| TIDF | Area $a$ | LFC | 1.7282 | 1.9127 | 1.9671 | - | - | - | 4.7603 | 204.7915 | - | - | - |
| | Area $b$ | LFC | 1.3983 | 0.036955 | 1.917 | - | - | - | 4.7358 | 83.0014 | - | - | - |

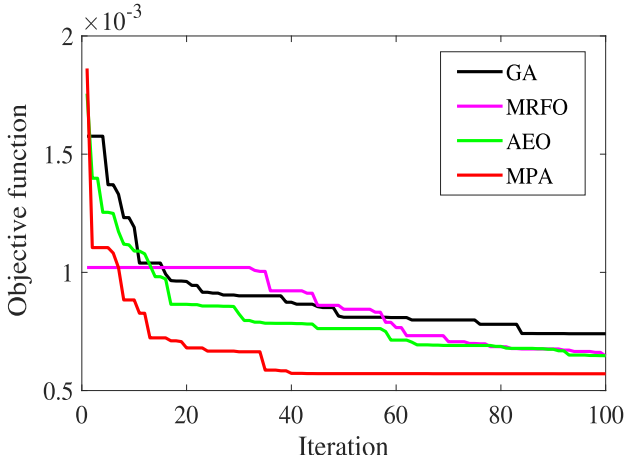


**FIGURE 6.** Convergence curve ISE at scenario 1 (case 1).

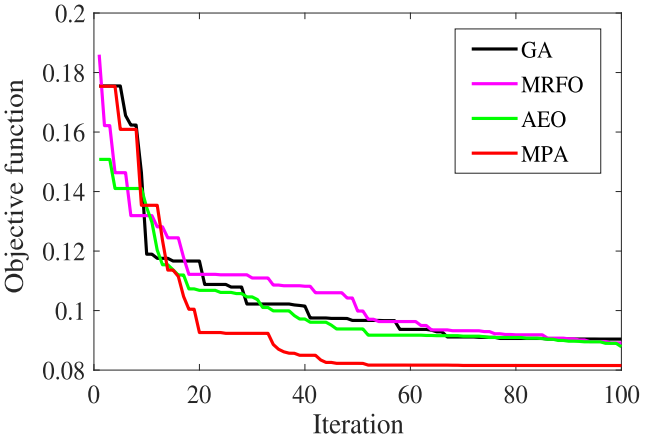


**FIGURE 7.** Convergence curve IAE at scenario 1 (case 1).

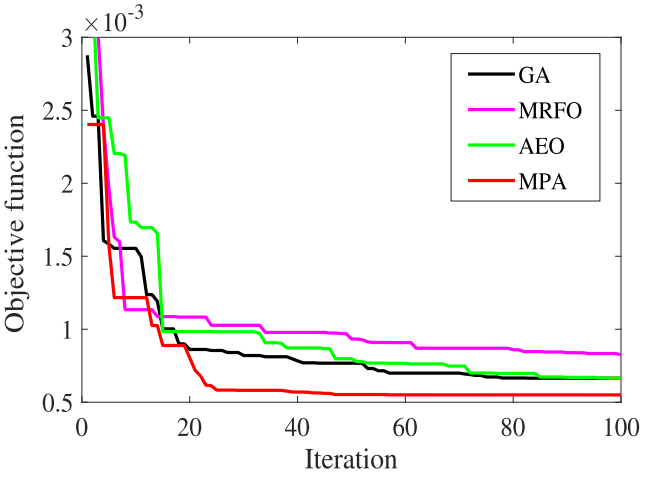


**FIGURE 8.** Convergence curve ITSE at scenario 1 (case 1).

interconnected power system model with considering different scenario operations of RESs penetrations and load variations. The evaluated cases are carried out using the MATLAB/SIMULINK programming code. The MPA is written in (.m file) and then it is interfaced with SIMULINK platform of the tested interconnected power system models to operate optimization processes. The main control parameters of the MPA are listed in Table 3. Moreover, the simulation results of the proposed controller are compared with the TIDF and HybFO controllers to investigate its superiority in terms of the percentage overshoot/undershoot in addition to settling times of frequency deviations following different cases of disturbances in the different scenarios.

### A. SCENARIO 1: LOADING CHANGES

The main objective of this scenario is to investigate the performance of the proposed HybFO-TIDF controller based on the MPA for the contribution of EVs in the interconnected power system stability by implementing step-load and high/low fluctuated loads. The convergence behavior of MPA is compared with different recent metaheuristic algorithms, such as genetic algorithm (GA), manta ray foraging optimization (MRFO) and artificial ecosystem optimization (AEO). Whereas, the various optimization algorithms are compared at the various objective functions, such as ISE, IAE, ITSE and ITAE. Fig. 6, Fig. 7, Fig. 8 and Fig. 9 show the convergence curves of the studied optimizers using the ISE, IAE, ITSE and ITAE methods, respectively. It can be clearly seen that MPA achieves the smallest error values and exhibits the fastest convergence under all of the calculated objectives.

This scenario is divided into three sub-scenarios of step load change, multiple load step changes and random loading variations as follows:

#### 1) STUDY CASE 1

In this case, the interconnected power system is tested against 5% step load changes at the initial time of simulation in area $b$. The frequency deviations of areas $a$ and $b$ are depicted in Fig. 10a and Fig. 10b, respectively. These figures show that the proposed controller provides lower peak values of the frequency, and the tie-line power deviation compared to the conventional TIDF and HybFO controllers. Moreover, Fig. 10c proves the superiority of the proposed combination controller. It can make the EVs discharge quickly the required power at the instant of

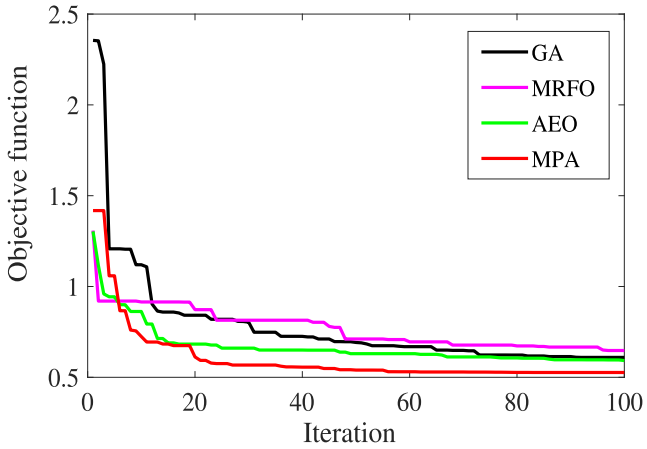


**FIGURE 9.** Convergence curve ITAE at scenario 1 (case 1).

disturbance and damps the tie-line power variation with low settling time and minimum overshoot compared to the TIDF and HybFO controllers as listed in Table 5.

### 2) STUDY CASE 2

In this case, the interconnected multi-area power system is subjected to two step-load disturbances, as shown in Fig. 11, with 5% in area *a* and 5% in area *b* at time t = 15s and 90s, respectively. In order to verify the robustness of the proposed LFC based on the optimized HybFO-TIDF combination controller, it is compared with the conventional TIDF and HybFO controllers individually. Fig. 12 shows the system frequency and tie-line power responses of the proposed system under the multi-step load changes. It is clear that the proposed combined controller exhibits more stable and rapid performance in restoring system frequency and tie-line power deviations compared to the other studied control techniques. It can be seen that the frequency deviation of the studied interconnected power system at t = 90s with the TIDF controller is about 0.038 Hz for area *a* and 0.052 Hz for area *b*. Whereas, the studied system with the HybFO controller gives the frequency deviation of about 0.035 Hz for area *a* and 0.05 Hz for area *b*. On the other hand, the proposed combination HybFO-TIDF control strategy succeeded at maintaining the frequency deviation with minimum undershoot of 0.01 Hz for area *a* and 0.022 Hz for area *b* during sudden load change. Furthermore, Fig. 12c shows that the tie-line power oscillation is damped quickly using the proposed controller compared to other traditional controllers. This, in turn, proves that the new coordination strategy of HybFO-TIDF combination controller and EVs delivers a significant amount of power to adapt the required power of the different sources.

### 3) STUDY CASE 3

In this case, the multi-area power system is examined under high random step and ramp load variations in area *a*, as shown in Fig. 13a, to investigate the robustness of the proposed combination HybFO-TIDF controller. It can be seen from Fig. 13b and Fig. 13c that the proposed coordinated strategy of LFC and EVs power-sharing based-on the optimized combination

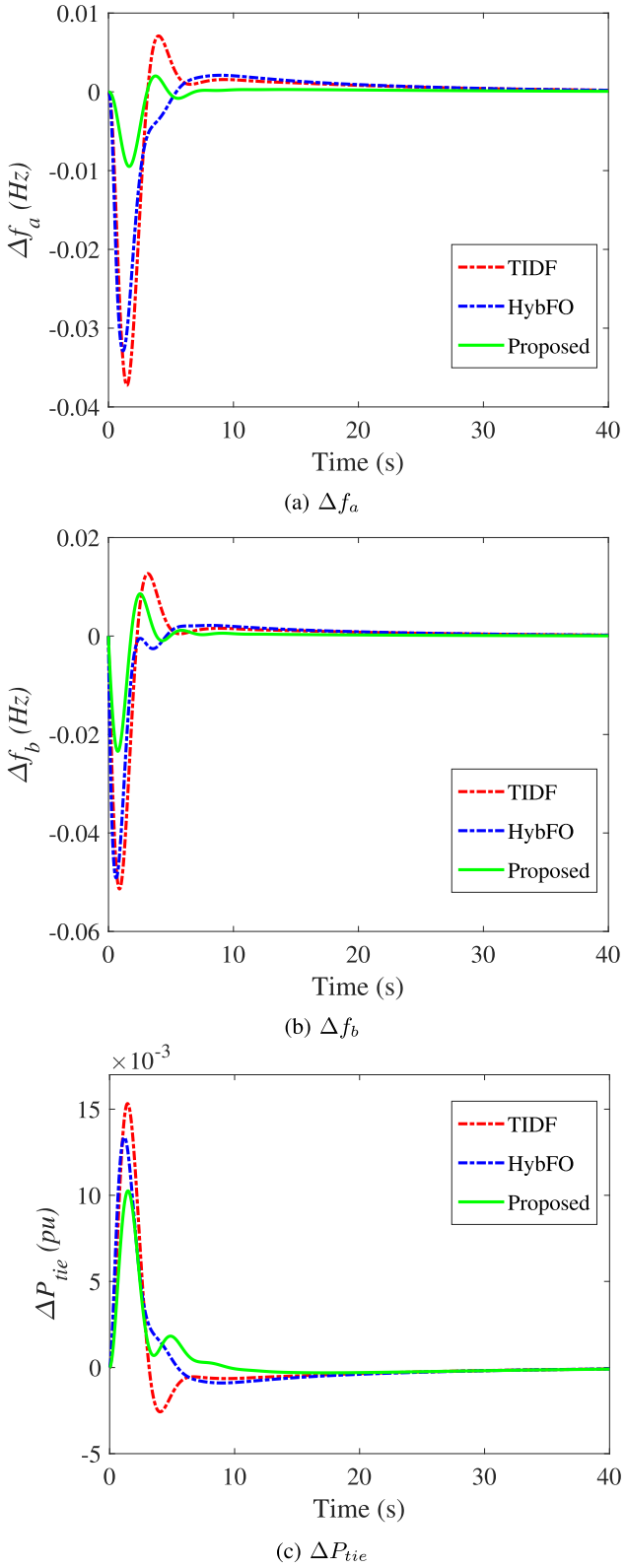


**FIGURE 10.** The dynamic response of system at scenario 1 (case 1).

controller can significantly enhance the system frequency stability in both areas. The proposed HybFO-TIDF can damp out the frequency deviations to lower values than the individual TIDF and HybFO, which has overshoot exceeds 0.1 Hz.

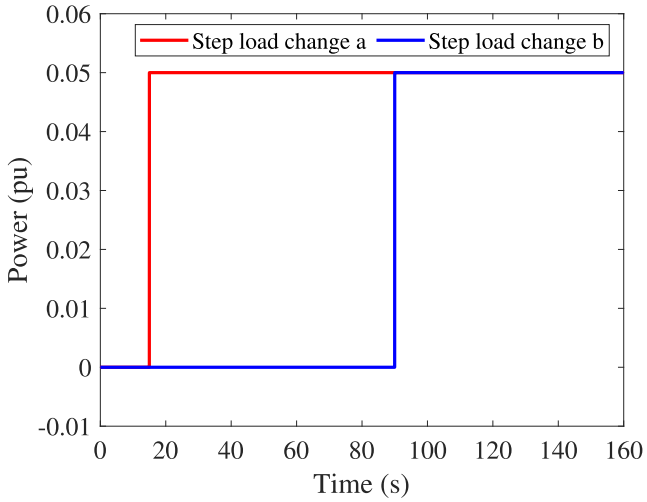


**FIGURE 11.** Generation profile for scenario 1 (case 2).

On the other hand, the tie-line power deviation between the two-area is regulated faster with less overshoot and undershoot values using the proposed controller compared to the other controllers as depicted in Fig. 13d. This proves the superiority of the proposed combination controller in the interconnected power systems over the conventional individual controllers in all cases of step load disturbances, multi-step disturbances and random load changes.

### B. SCENARIO 2: RESs DISORDERS

This case is targeted to demonstrate the effectiveness of the proposed strategy of the parallel combination of HybFO-TIDF and contribution of EVs on the dynamic response of the interconnected multi-area power system under disorders in RESs. The studied system is incurred to the intermittent nature and fluctuations of RESs, such as wind and PV generations. The two sources are classified as the important components of interconnected power systems, especially in microgrids. In this scenario, the suggested coordination of LFC and EVs using the optimized HybFO-TIDF controller based on MPA is tested under a severe condition of load and RESs variations. In which, the PV generation unit is inserted to the interconnected power systems at time = 10s at area *b*, wind generation unit is inserted at time = 70s at area *a*, and a sudden step-load of 5% at time = 40s at area *b* is inserted as shown in Fig. 14.

It is clear from Fig. 15 that utilizing the conventional TIDF and HybFO controllers can restore the system frequency and the tie-line power deviations but with long settling time and high overshoot and undershoot values of more than ±0.1Hz at the instants of PV and wind connections. However, the proposed technique succeeded in damping out the frequency deviations to values less than 0.05Hz and 0.04Hz in areas *a* and *b*, respectively. As well, the tie-line power is varied to be less than 0.02p.u at wind integration. This case proves the merits of the combined HybFO-TIDF controller as the FO integral, and the derivative terms have the ability to reduce settling time with the proposed controller. In addition,

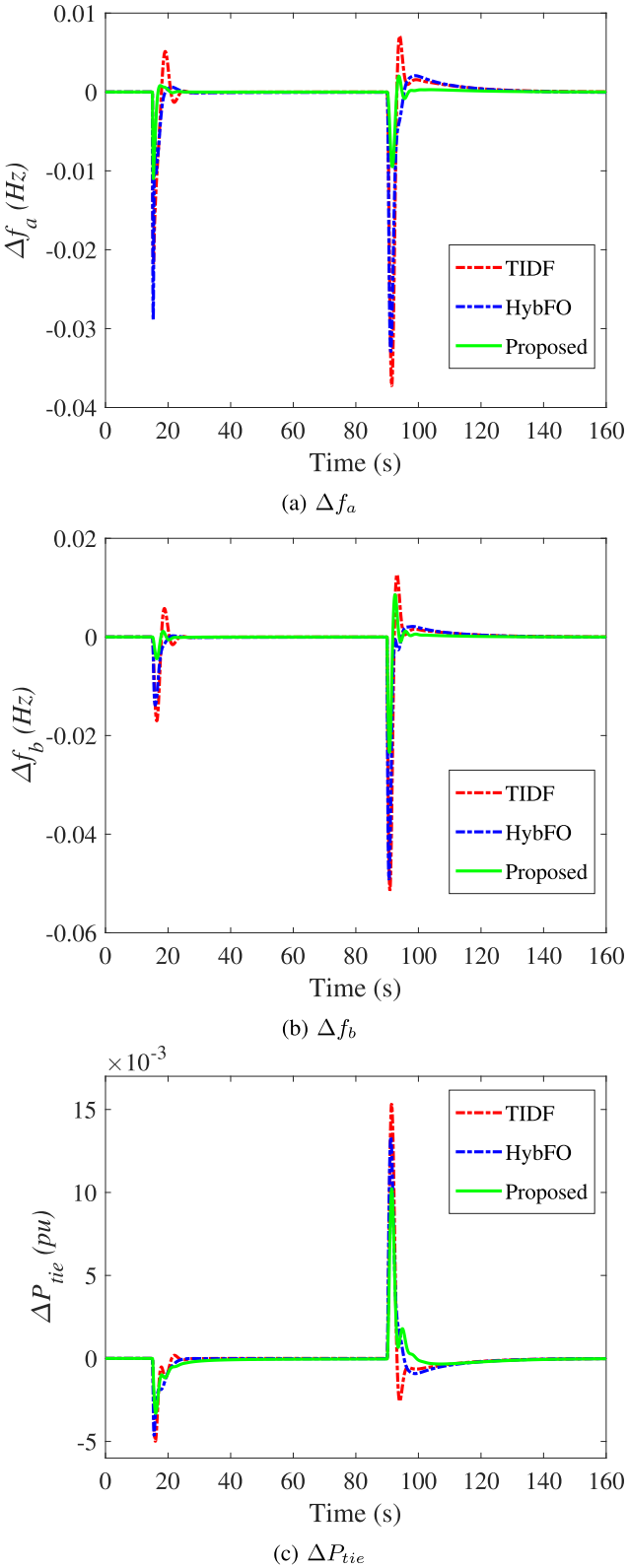


**FIGURE 12.** System dynamic responses at scenario 1 (case 2).

combining the FO derivative term to the integral term result in the enrichment of TIDF controller with higher DoF than the integral, and the derivative terms. Moreover, it has become obvious that the proposed controller based on the MPA

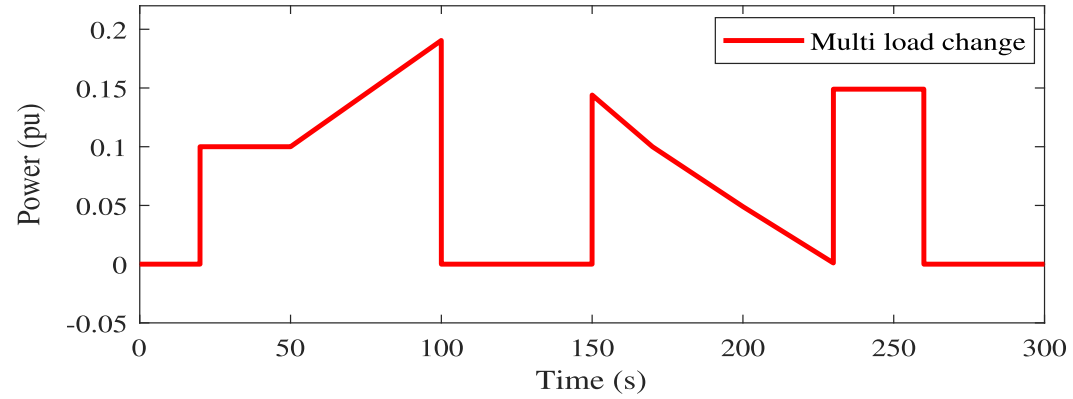


(a) The generation and load waveforms for scenario 1 (case 3).

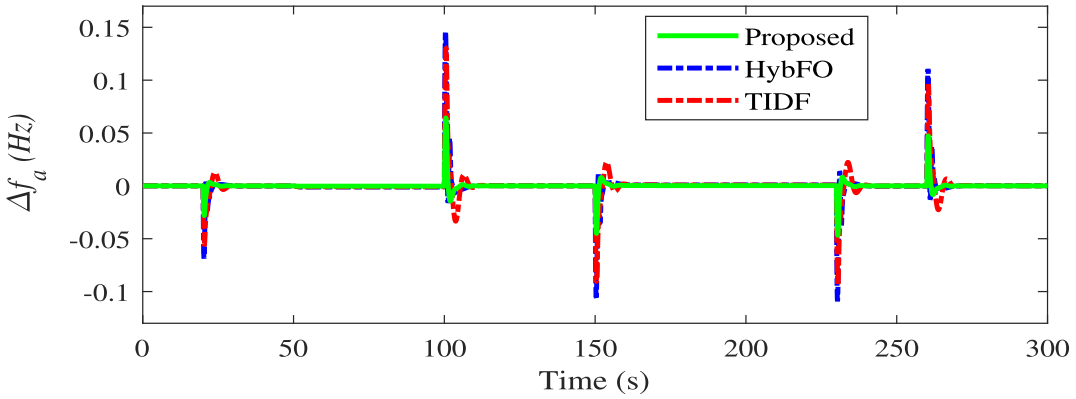


(b) $\Delta f_a$

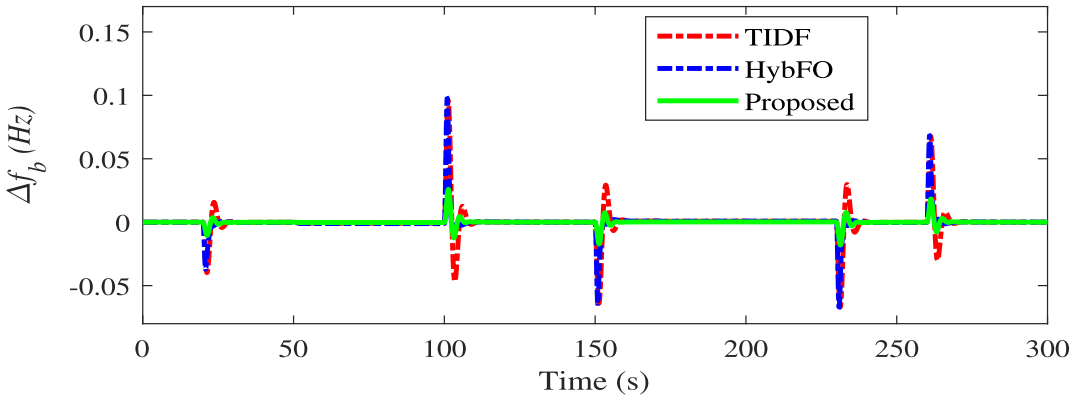


(c) $\Delta f_b$

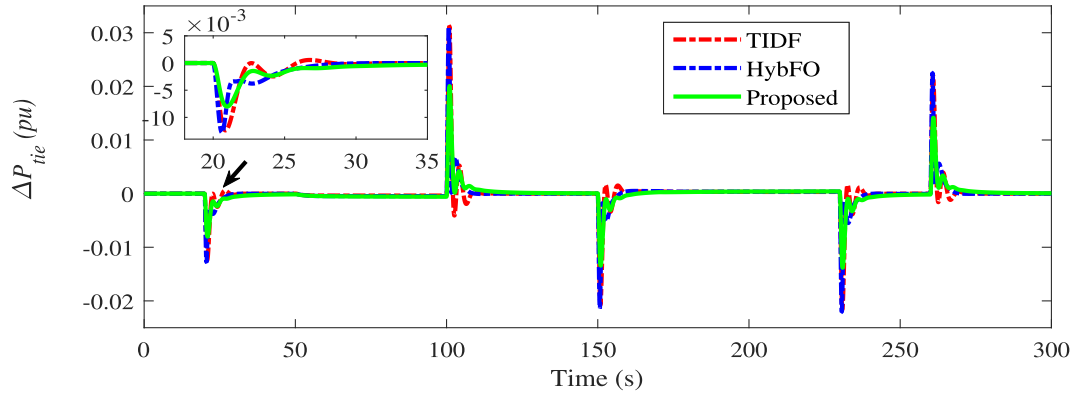


(d) $\Delta P_{tie}$

**FIGURE 13.** System response with the optimized controllers at scenario 1 (case 3).

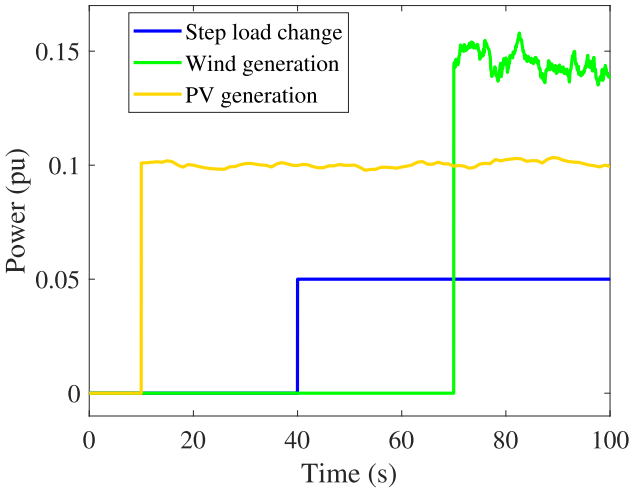


**FIGURE 14.** Generation and load profiles for scenario 2.

technique enables proper cooperation among the LFC and the EV systems. The generated powers in area $a$ and area $b$ for this scenario are shown in Fig. 16 and Fig. 17, respectively. It can be seen from these figures that each area has increased its generation to cover its load demand in order to regulate the tie-line power at zero value.

### C. SCENARIO 3: HIGH RESs PENETRATION

In order to investigate the performance of the system with extreme change in the studied system, it is operated under the situation of high penetration levels of RESs. Wherein, the PV generation is connected from initial time of simulation at area $b$, wind generation is connected at time $=$ 80s at area $a$, wind generation is connected at time $=$ 40s at area $b$, and 5% of step load from the initial time in both areas $a$ and $b$ as shown in Fig. 18a. It can be seen from Fig. 18b and Fig. 18c that the proposed combined HybFO-TIDF controller demonstrates superior dynamic performance compared with the other traditional TIDF and HybFO controllers in terms of a perceptible reduction in settling time, undershoot, and overshoot. It is also observed that the proposed controller enables the EVs to cooperate in injecting sufficient power to the system so as to obtain fast and stable performance as depicted in the tie-line power waveform of Fig. 18d. Whereas, the TIDF and HybFO controllers do not have the capability to deliver the same amount of power to the system and it needs to compensate the lack of power from the thermal or hydraulic generation units.

### D. SCENARIO 4: RESs DISORDERS AND SYSTEM UNCERTAINTIES

For real-time applications, the robustness of the proposed parallel combination of HybFO-TIDF controller is analyzed for the interconnected power system with system parameters uncertainties. In this scenario, the studied power system is operated at the same conditions of scenario 2 with 35% reduction of system inertia and with varying all system parameters with the same percentage. This scenario is

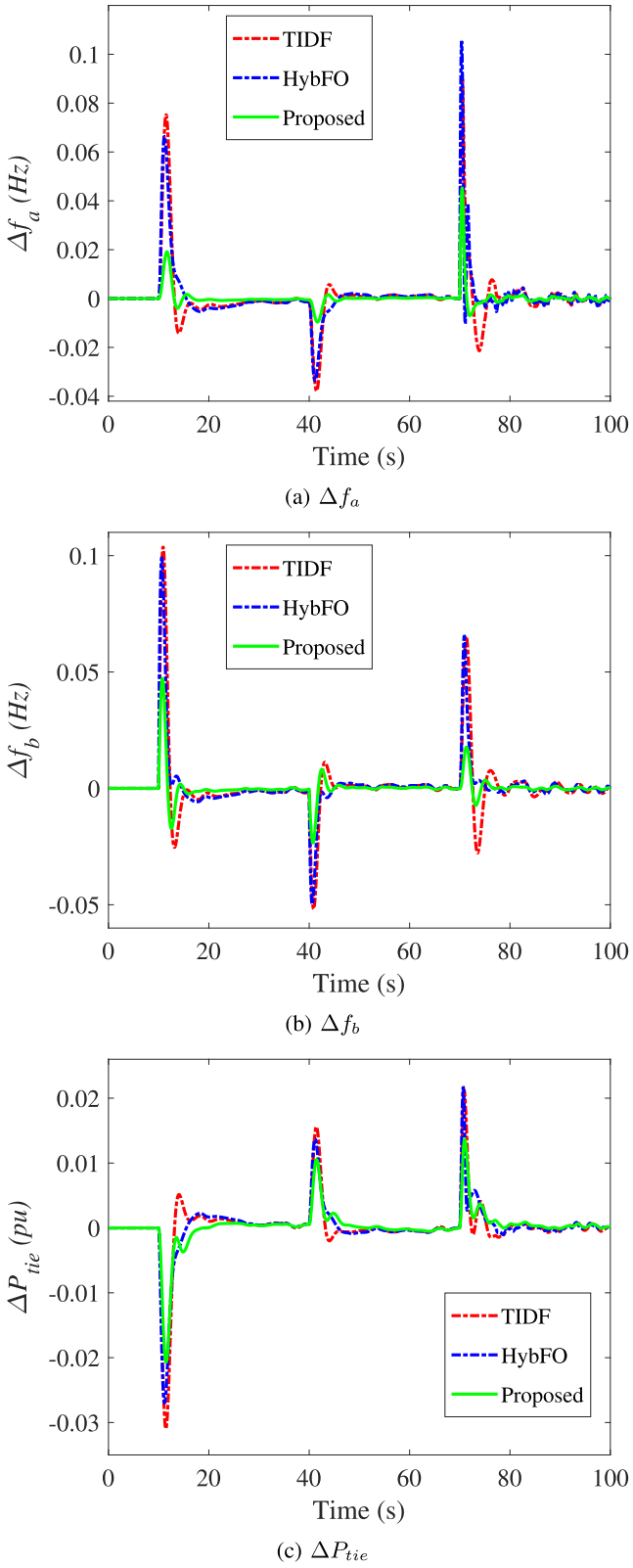


**FIGURE 15.** System dynamic response at scenario 2.

performed to verify the stability of power systems under different uncertainty conditions. Fig. 19 shows the dynamic responses of the studied system in terms of both of the frequency and the tie-line power fluctuations. It can be noted

**TABLE 4.** Comparative analysis of Performance indices for the different cases study.

| Scenario | Controller technique | Performance indices | | | |
|---|---|---|---|---|---|
| | | ISE | IAE | ITSE | ITAE |
| No.1 (Case 1) | TIDF | 0.0052 | 0.2665 | 0.0077 | 1.7986 |
| | HybFO | 0.0034 | 0.1941 | 0.0036 | 1.6180 |
| | Proposed | 0.00080721 | 0.1022 | 0.0011 | 0.7058 |
| No.1 (Case 2) | TIDF | 0.0061 | 0.3608 | 0.4914 | 27.4552 |
| | HybFO | 0.0040 | 0.3063 | 0.3193 | 23.2934 |
| | Proposed | 0.00091726 | 0.1398 | 0.0755 | 10.8304 |
| No.1 (Case 3) | TIDF | 0.0707 | 1.9643 | 11.2811 | 311.4987 |
| | HybFO | 0.0557 | 1.6513 | 8.9093 | 256.0460 |
| | Proposed | 0.0100 | 0.7193 | 1.5950 | 113.4969 |
| No.2 | TIDF | 0.0393 | 1.1654 | 1.3723 | 49.0647 |
| | HybFO | 0.0277 | 0.8575 | 1.0323 | 36.7878 |
| | Proposed | 0.0059 | 0.4356 | 0.1984 | 17.8915 |
| No.3 | TIDF | 0.0765 | 1.8802 | 3.7914 | 110.8869 |
| | HybFO | 0.0504 | 1.3799 | 2.4773 | 78.9702 |
| | Proposed | 0.0119 | 0.7314 | 0.5508 | 40.6772 |
| No.4 | TIDF | 0.0363 | 1.1047 | 1.2116 | 45.6839 |
| | HybFO | 0.0266 | 0.8905 | 0.9646 | 37.5513 |
| | Proposed | 0.0054 | 0.4198 | 0.1753 | 16.9800 |

**TABLE 5.** Settling times (ST), maximum undershoots (MU), and maximum overshoots (MO) at various studied scenarios.

| Scenario | Controller | $\Delta f_a$ | | | $\Delta f_b$ | | | $\Delta P_{tie}$ | | |
|---|---|---|---|---|---|---|---|---|---|---|
| | | MO | MU | ST | MO | MU | ST | MO | MU | ST |
| No.1 (Case 1) (at initial time) | TIDF | - | 0.03725 | 31 | - | 0.05129 | 34.32 | 0.01532 | - | 26 |
| | HybFO | - | 0.03287 | 27 | - | 0.04912 | 28.12 | 0.01334 | - | 21 |
| | Proposed | - | 0.00946 | 22 | - | 0.02331 | 23.04 | 0.01025 | - | 15 |
| No.1 (Case 2) (at 90s) | TIDF | 0.007023 | 0.03719 | 137 | 0.001238 | 0.05103 | 146 | 0.01527 | 0.002428 | 117 |
| | HybFO | 0.002063 | 0.03267 | 123 | 0.002121 | 0.04884 | 125 | 0.01323 | 0.0009059 | 112 |
| | Proposed | 0.001923 | 0.009199 | 114 | 0.008227 | 0.02294 | 110 | 0.01012 | - | 107 |
| No.1 (Case 3) (at 150s) | TIDF | 0.02237 | 0.1056 | 174 | 0.0291 | 0.06363 | 181 | 0.001626 | 0.02078 | 181 |
| | HybFO | 0.01236 | 0.09089 | 168 | - | 0.06437 | 174 | - | 0.02135 | 175 |
| | Proposed | 0.00782 | 0.04502 | 162 | 0.007339 | 0.0172 | 169 | - | 0.01321 | 172 |
| No. 2 (at 40s) | TIDF | 0.005703 | 0.03784 | 52.9 | 0.01124 | 0.05181 | 52.2 | 0.01558 | 0.001987 | 52.8 |
| | HybFO | 0.002063 | 0.03293 | 53.4 | 0.002128 | 0.04943 | 52.7 | 0.01367 | 0.0006513 | 53.6 |
| | Proposed | 0.001629 | 0.009515 | 48.6 | 0.008149 | 0.02322 | 47.4 | 0.01052 | - | 51.5 |
| No. 3 (at 40s) | TIDF | 0.1211 | 0.02487 | 55.6 | 0.1669 | 0.003351 | 51.3 | 0.008884 | 0.04981 | 55.6 |
| | HybFO | 0.1067 | 0.006161 | 57.6 | 0.1578 | 0.04402 | 47.5 | 0.002482 | 0.04321 | 57 |
| | Proposed | 0.03 | 0.006493 | 47.5 | 0.07559 | 0.02864 | 45.2 | - | 0.03301 | 49.2 |
| No. 4 (at 70s) | TIDF | 0.08363 | 0.01732 | 78 | 0.05976 | 0.02138 | 80.04 | 0.01961 | - | 83.9 |
| | HybFO | 0.1003 | 0.0104 | 75.9 | 0.05986 | 0.0006217 | 79.7 | 0.0202 | - | 81.7 |
| | Proposed | 0.04281 | 0.004602 | 75.7 | 0.01618 | 0.005385 | 77.1 | 0.01246 | - | 78.8 |

* ST denotes to settle time in seconds

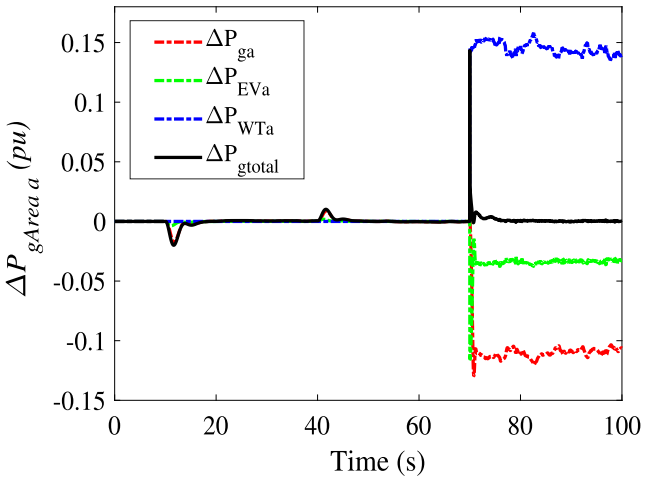


**FIGURE 16.** Power generations of area *a* at scenario 2.

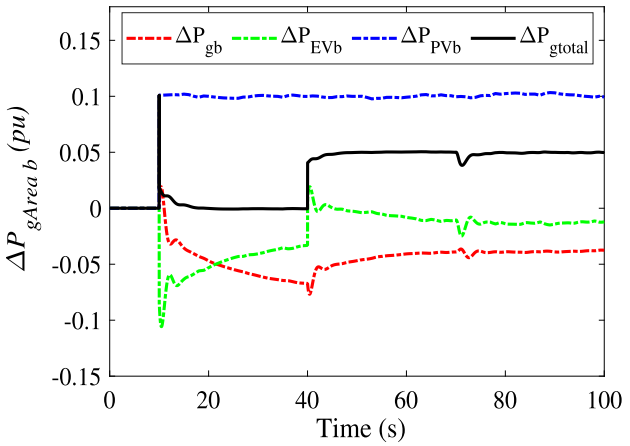


**FIGURE 17.** Power generations of area *b* at scenario 2.

that the conventional TIDF and HybFO controllers fail to damp out the high overshoot of the frequency deviations, which exceed the allowable limits (±0.1 Hz). However, the proposed HybFO-TIDF controller makes the coordination of LFC and EVs capable of achieving improved frequency regulations as well as the tie-line power control. Therefore, the proposed combined controller has a robust performance

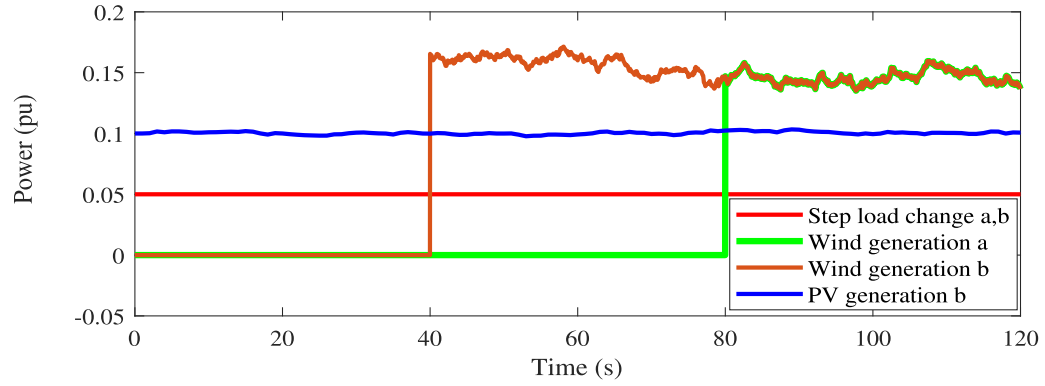


(a) The generation and load waveforms for scenario 3.

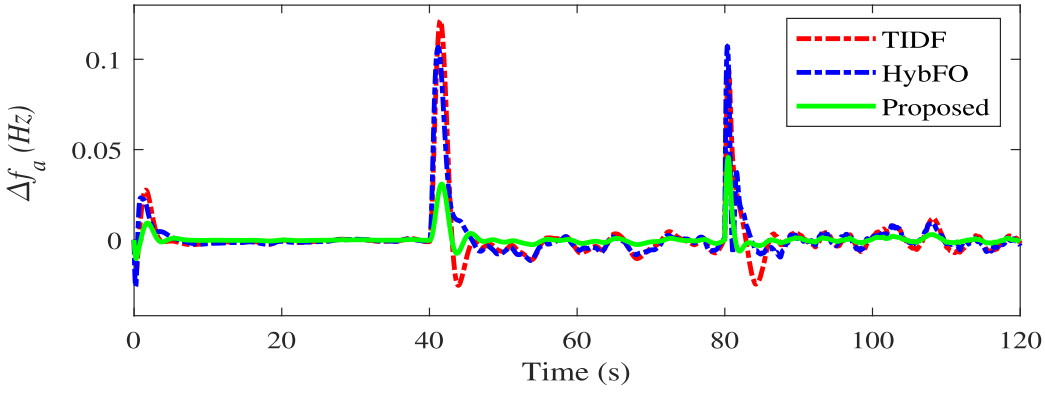


(b) $\Delta f_a$

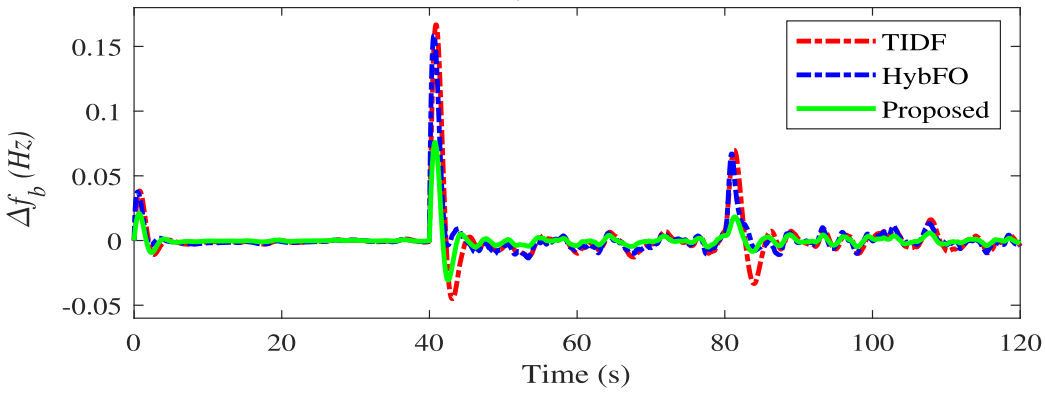


(c) $\Delta f_b$

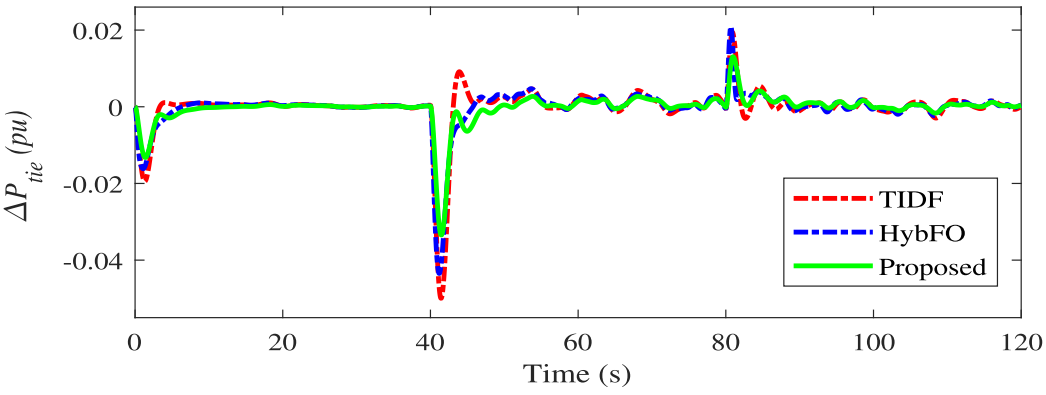


(d) $\Delta P_{tie}$

**FIGURE 18.** System response with the optimized controllers at scenario 3.

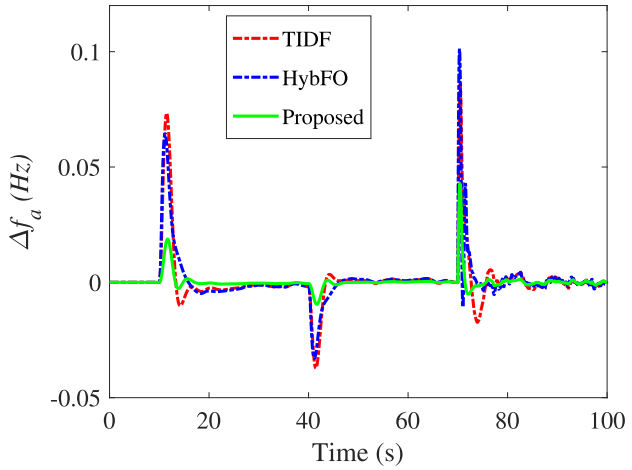


(a) $\Delta f_a$

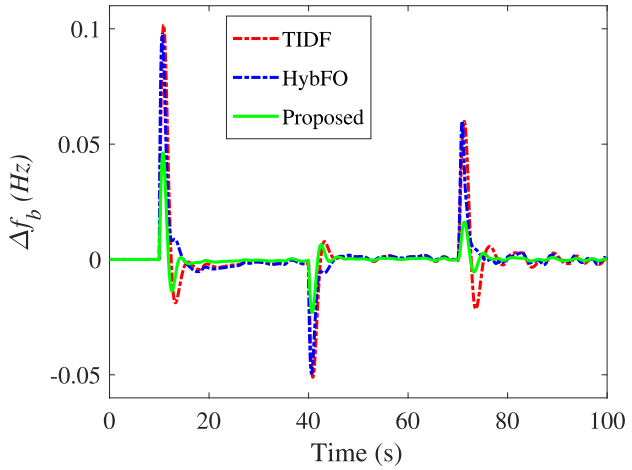


(b) $\Delta f_b$

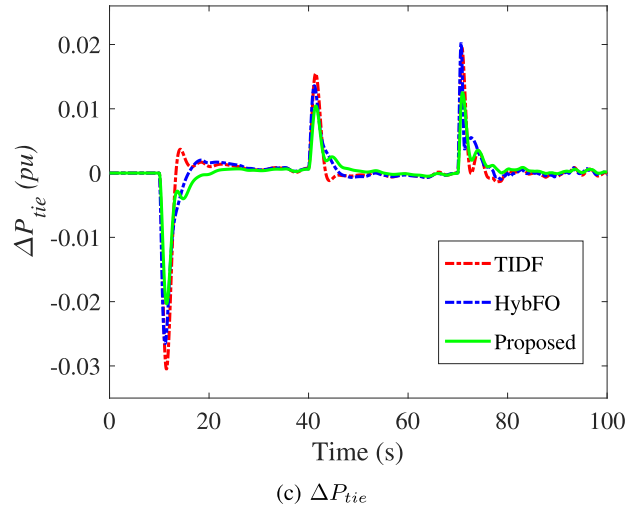


(c) $\Delta P_{tie}$

**FIGURE 19.** System dynamic response with system parameters variations at scenario 4.

with the coordination of LFC and contribution of EVs. Furthermore, the proposed controller has the ability to perform LFC action efficiently in case of different disturbances and uncertainties, which are very common in the actual operation of an interconnected multi-area power system.

## VI. PERFORMANCE COMPARISON

Different performance indices are calculated for the studied controllers as tabulated in Table 4. The comparison includes ISE, IAE, ITSE and ITAE values for the different studied cases. Table 4 shows that the proposed controller can achieve improved values for all calculated performance indices in various system scenarios. Moreover, the evaluated performance indices illustrate the superiority of the proposed controller over the traditional controllers. For example, in scenario 1 (case 1), the ISE values are 0.0052, 0.0034 and 0.00080721 for the TIDF, HybFO, and proposed HybFO-TIDF controllers, respectively. It can be also observed that the calculated ISE values under the proposed control method is 15.52%, and 23.74% of the ISE values under the TIDF, and HybFO controllers, respectively. Furthermore, the IAE values are 0.2665, 0.1941 and 0.1022 for the TIDF, HybFO and proposed control, respectively. Whereas, the IAE values for proposed control are 38.35%, and 52.65% of the IAE values with TIDF, and HybFO controllers, respectively. The situation is the same for the ITSE and ITAE. To sum up, the proposed controller achieves the best performance indices compared to the other addressed controllers. These performance indices prove the superiority of the proposed controller in all the studied scenarios at various performance objectives.

## VII. CONCLUSION

In this paper, a new combination of fractional-order control systems is proposed for two-area interconnected power systems. The proposed controller combines TIDF and HybFO controllers to improve power system stability during frequency and tie-line power fluctuations. The proposed controller achieved the following benefits:

- A two-degree of freedom (2-DOF) controller has been proposed by combining the merits of both controllers (HybrFO and TIDF). The first feedback signal uses the ACE, which enables the proposed controller to mitigate the low-frequency oscillations. Whereas, the second feedback signal uses the frequency deviation, which is being responsible for mitigating the high-frequency signal.
- An optimized design algorithm for the controller parameters is achieved by using the new recent MPA algorithm, which enables the simultaneous determination of the optimum control parameters. The used MPA in designing the controller parameters presents the best convergence rate in all error estimation methods compared to the other optimization algorithms, such as GA, MRFO and EOA algorithms.
- The coordination of the power system generations and installed EVs is achieved to incorporate additional functionalities for future extensions of EVs in electrical power systems.
- The obtained results of the studied system with high penetration levels of RESs confirm the superiority of the proposed combined controller and the design method over the traditional addressed methods.

- Compared to traditional TIDF controllers, the proposed controller and design algorithm achieve 15.52%, and 38.35% of the ISE and IAE values. Additionally, the proposed controller has 23.74%, and 52.65% of the ISE and IAE values under the HybFO controller, respectively.

## REFERENCES

[1] S. M. Said, M. Aly, B. Hartmann, A. G. Alharbi, and E. M. Ahmed, "SMES-based fuzzy logic approach for enhancing the reliability of microgrids equipped with PV generators," *IEEE Access*, vol. 7, pp. 92059–92069, 2019.

[2] S. M. Said, M. Aly, and H. Balint, "An efficient reactive power dispatch method for hybrid photovoltaic and superconducting magnetic energy storage inverters in utility grids," *IEEE Access*, vol. 8, pp. 183708–183721, 2020.

[3] A. Latif, S. M. S. Hussain, D. C. Das, T. S. Ustun, and A. Iqbal, "A review on fractional order (FO) controllers' optimization for load frequency stabilization in power networks," *Energy Rep.*, vol. 7, pp. 4009–4021, Nov. 2021.

[4] S. Oshnoei, A. Oshnoei, A. Mosallanejad, and F. Haghjoo, "Contribution of GCSC to regulate the frequency in multi-area power systems considering time delays: A new control outline based on fractional order controllers," *Int. J. Electr. Power Energy Syst.*, vol. 123, Dec. 2020, Art. no. 106197.

[5] H. A. Yousef, K. AL-Kharusi, M. H. Albadi, and N. Hosseinzadeh, "Load frequency control of a multi-area power system: An adaptive fuzzy logic approach," *IEEE Trans. Power Syst.*, vol. 29, no. 4, pp. 1822–1830, Jul. 2014.

[6] S. Debbarma and A. Dutta, "Utilizing electric vehicles for LFC in restructured power systems using fractional order controller," *IEEE Trans. Smart Grid*, vol. 8, no. 6, pp. 2554–2564, Nov. 2017.

[7] M. Dreidy, H. Mokhlis, and S. Mekhilef, "Inertia response and frequency control techniques for renewable energy sources: A review," *Renew. Sustain. Energy Rev.*, vol. 69, pp. 144–155, Mar. 2017.

[8] S. K. Pandey, S. R. Mohanty, and N. Kishor, "A literature survey on load–frequency control for conventional and distribution generation power systems," *Renew. Sustain. Energy Rev.*, vol. 25, pp. 318–334, Sep. 2013.

[9] R. Shankar, S. R. Pradhan, K. Chatterjee, and R. Mandal, "A comprehensive state of the art literature survey on LFC mechanism for power system," *Renew. Sustain. Energy Rev.*, vol. 76, pp. 1185–1207, Sep. 2017.

[10] J. Nanda, M. Sreedhar, and A. Dasgupta, "A new technique in hydro thermal interconnected automatic generation control system by using minority charge carrier inspired algorithm," *Int. J. Electr. Power Energy Syst.*, vol. 68, pp. 259–268, Jun. 2015.

[11] K. Singh, M. Amir, F. Ahmad, and M. A. Khan, "An integral tilt derivative control strategy for frequency control in multimicrogrid system," *IEEE Syst. J.*, vol. 15, no. 1, pp. 1477–1488, Mar. 2021.

[12] A. Khalil, Z. Rajab, A. Alfergani, and O. Mohamed, "The impact of the time delay on the load frequency control system in microgrid with plug-in-electric vehicles," *Sustain. Cities Soc.*, vol. 35, pp. 365–377, Nov. 2017.

[13] J. Sharma, Y. V. Hote, and R. Prasad, "PID controller design for interval load frequency control system with communication time delay," *Control Eng. Pract.*, vol. 89, pp. 154–168, Aug. 2019.

[14] D. Yousri, T. S. Babu, and A. Fathy, "Recent methodology based Harris hawks optimizer for designing load frequency control incorporated in multi-interconnected renewable energy plants," *Sustain. Energy, Grids Netw.*, vol. 22, Jun. 2020, Art. no. 100352.

[15] A. Oshnoei, R. Khezri, S. M. Muyeen, S. Oshnoei, and F. Blaabjerg, "Automatic generation control incorporating electric vehicles," *Electr. Power Compon. Syst.*, vol. 47, no. 8, pp. 720–732, May 2019.

[16] E. M. Ahmed, E. A. Mohamed, A. Elmelegi, M. Aly, and O. Elbaksawi, "Optimum modified fractional order controller for future electric vehicles and renewable energy-based interconnected power systems," *IEEE Access*, vol. 9, pp. 29993–30010, 2021.

[17] G. Magdy, A. Bakeer, M. Nour, and E. Petlenkov, "A new virtual synchronous generator design based on the SMES system for frequency stability of low-inertia power grids," *Energies*, vol. 13, no. 21, p. 5641, Oct. 2020.

[18] Y. Arya, "Impact of ultra-capacitor on automatic generation control of electric energy systems using an optimal FFOID controller," *Int. J. Energy Res.*, vol. 43, pp. 8765–8778, Aug. 2019.

[19] S. Priyadarshani, K. R. Subhashini, and J. K. Satapathy, "Pathfinder algorithm optimized fractional order tilt-integral-derivative (FOTID) controller for automatic generation control of multi-source power system," *Microsyst. Technol.*, vol. 27, no. 1, pp. 23–35, Jun. 2020.

[20] A. Fathy and A. G. Alharbi, "Recent approach based movable damped wave algorithm for designing fractional-order PID load frequency control installed in multi-interconnected plants with renewable energy," *IEEE Access*, vol. 9, pp. 71072–71089, 2021.

[21] M. S. Ayas and E. Sahin, "FOPID controller with fractional filter for an automatic voltage regulator," *Comput. Electr. Eng.*, vol. 90, Mar. 2021, Art. no. 106895.

[22] Y. Arya, "Effect of electric vehicles on load frequency control in interconnected thermal and hydrothermal power systems utilising CF-FOIDF controller," *IET Gener., Transmiss. Distrib.*, vol. 14, no. 14, pp. 2666–2675, May 2020.

[23] A. Zamani, S. M. Barakati, and S. Yousofi-Darmian, "Design of a fractional order PID controller using GBMO algorithm for load–frequency control with governor saturation consideration," *ISA Trans.*, vol. 64, pp. 56–66, Sep. 2016.

[24] J. R. Nayak, B. Shaw, and B. K. Sahu, "Implementation of hybrid SSA–SA based three-degree-of-freedom fractional-order PID controller for AGC of a two-area power system integrated with small hydro plants," *IET Gener., Transmiss. Distrib.*, vol. 14, no. 13, pp. 2430–2440, May 2020.

[25] S. R. Kumar, S. Panda, A. Biswal, and G. T. C. Sekhar, "Design and analysis of tilt integral derivative controller with filter for load frequency control of multi-area interconnected power systems," *ISA Trans.*, vol. 61, pp. 251–264, Mar. 2016.

[26] S. Malik and S. Suhag, "A novel SSA tuned PI-TDF control scheme for mitigation of frequency excursions in hybrid power system," *Smart Sci.*, vol. 8, no. 4, pp. 202–218, Sep. 2020.

[27] A. Latif, S. M. S. Hussain, D. C. Das, and T. S. Ustun, "Optimum synthesis of a BOA optimized novel dual-stage PI–(1 + ID) controller for frequency response of a microgrid," *Energies*, vol. 13, no. 13, p. 3446, Jul. 2020.

[28] E. A. Mohamed, E. M. Ahmed, A. Elmelegi, M. Aly, O. Elbaksawi, and A.-A.-A. Mohamed, "An optimized hybrid fractional order controller for frequency regulation in multi-area power systems," *IEEE Access*, vol. 8, pp. 213899–213915, 2020.

[29] Y. Arya, "A novel CFFOPI-FOPID controller for AGC performance enhancement of single and multi-area electric power systems," *ISA Trans.*, vol. 100, pp. 126–135, May 2020.

[30] Y. Arya, N. Kumar, P. Dahiya, G. Sharma, E. Çelik, S. Dhundhara, and M. Sharma, "Cascade-I $^{\lambda}$D$^{\mu}$N controller design for AGC of thermal and hydro-thermal power systems integrated with renewable energy sources," *IET Renew. Power Gener.*, vol. 15, no. 3, pp. 504–520, Jan. 2021.

[31] Y. A. Dahab, H. Abubakr, and T. H. Mohamed, "Adaptive load frequency control of power systems using electro-search optimization supported by the balloon effect," *IEEE Access*, vol. 8, pp. 7408–7422, 2020.

[32] Y. Arya, N. Kumar, P. Dahiya, G. Sharma, E. Çelik, S. Dhundhara, and M. Sharma, "Cascade-I$^{\lambda}$D$^{\mu}$N controller design for AGC of thermal and hydro-thermal power systems integrated with renewable energy sources," *IET Renew. Power Gener.*, vol. 15, no. 3, pp. 504–520, Jan. 2021.

[33] M. Elsisi, M. Soliman, M. A. S. Aboelela, and W. Mansour, "Model predictive control of plug-in hybrid electric vehicles for frequency regulation in a smart grid," *IET Gener., Transmiss. Distrib.*, vol. 11, no. 16, pp. 3974–3983, Oct. 2017.

[34] H. H. Ali, A. Fathy, and A. M. Kassem, "Optimal model predictive control for LFC of multi-interconnected plants comprising renewable energy sources based on recent sooty terns approach," *Sustain. Energy Technol. Assessments*, vol. 42, Dec. 2020, Art. no. 100844.

[35] H. H. Ali, A. M. Kassem, M. Al-Dhaifallah, and A. Fathy, "Multi-verse optimizer for model predictive load frequency control of hybrid multi-interconnected plants comprising renewable energy," *IEEE Access*, vol. 8, pp. 114623–114642, 2020.

[36] A. Bagheri, A. Jabbari, and S. Mobayen, "An intelligent ABC-based terminal sliding mode controller for load-frequency control of islanded micro-grids," *Sustain. Cities Soc.*, vol. 64, Jan. 2021, Art. no. 102544.

[37] J. Guo, "Application of full order sliding mode control based on different areas power system with load frequency control," *ISA Trans.*, vol. 92, pp. 23–34, Sep. 2019.

[38] N. Jalali, H. Razmi, and H. Doagou-Mojarrad, "Optimized fuzzy self-tuning PID controller design based on tribe-DE optimization algorithm and rule weight adjustment method for load frequency control of interconnected multi-area power systems," *Appl. Soft Comput.*, vol. 93, Aug. 2020, Art. no. 106424.

[39] S. Falahati, S. A. Taher, and M. Shahidehpour, "Grid secondary frequency control by optimized fuzzy control of electric vehicles," *IEEE Trans. Smart Grid*, vol. 9, no. 6, pp. 5613–5621, Nov. 2018.
[40] A. H. Yakout, H. Kotb, H. M. Hasanien, and K. M. Aboras, "Optimal fuzzy PIDF load frequency controller for hybrid microgrid system using Marine predator algorithm," *IEEE Access*, vol. 9, pp. 54220–54232, 2021.
[41] M. A. Sobhy, A. Y. Abdelaziz, H. M. Hasanien, and M. Ezzat, "Marine predators algorithm for load frequency control of modern interconnected power systems including renewable energy sources and energy storage units," *Ain Shams Eng. J.*, early access, Jun. 2021.
[42] A. H. Yakout, M. A. Attia, and H. Kotb, "Marine predator algorithm based cascaded PIDA load frequency controller for electric power systems with wave energy conversion systems," *Alexandria Eng. J.*, vol. 60, no. 4, pp. 4213–4222, Aug. 2021.
[43] M. Aly, E. M. Ahmed, H. Rezk, and E. A. Mohamed, "Marine predators algorithm optimized reduced sensor fuzzy-logic based maximum power point tracking of fuel cell-battery standalone applications," *IEEE Access*, vol. 9, pp. 27987–28000, 2021.
[44] A. Faramarzi, M. Heidarinejad, S. Mirjalili, and A. H. Gandomi, "Marine predators algorithm: A nature-inspired Metaheuristic," *Expert Syst. Appl.*, vol. 152, Aug. 2020, Art. no. 113377.

**EMAD M. AHMED** (Senior Member, IEEE) received the B.Sc. and M.Sc. degrees from Aswan University, Egypt, in 2001 and 2006, respectively, and the Ph.D. degree from Kyushu University, Japan, in 2012.

He joined Aswan Power Electronics Applications Research Center (APEARC), from 2012 to 2018. In 2018, he joined Aswan Wireless Communication Research Center (AWCRC). He is currently working as an Associate Professor with the Department of Electrical Engineering, Faculty of Engineering, Aswan University. Moreover, he is on a leave with the Faculty of Engineering, Jouf University, Saudi Arabia. His present research interests include applied power electronics, especially in renewable energy applications, micro-grids, fault tolerant control, and battery management systems, electric vehicles, and LED drivers.

He is a member of the IEEE Power Electronics Society (PELS), the IEEE Industrial Electronics Society (IES), and the IEEE Power and Energy Society (PES).

**AHMED ELMELEGI** received the B.Sc. and M.Sc. degrees in electrical power engineering from Aswan University, Aswan, Egypt, in 2005 and 2019, respectively. He has been with Upper Egypt Electricity Distribution Company, Ministry of Electricity and Renewable Energy, Aswan, since 2007. His current research interests include applied power electronics in renewable energy applications, multi-level inverters, and micro-grids.

**AHMED SHAWKY** (Member, IEEE) was born in Aswan, Egypt, in 1988. He received the B.Sc. and M.Sc. degrees in electrical engineering from the Faculty of Engineering and Technology, Aswan University, Aswan, in 2010 and 2014, respectively, and the Ph.D. degree in electrical engineering from Nagoya Institute of Technology, Nagoya, Japan, in 2021. He worked at Aswan Power Electronic Application Research Center (APEARC), as an Assistant Researcher, in 2010, and appointed as a Team Leader of the System Group, in early 2012. Since 2011, he has been with the Department of Electrical Engineering and Technology, Aswan University, first as an Administrator in 2011, and a Lecturer Assistant in 2014. He has been an Assistant Professor with the Department of Electrical Engineering and Technology, Aswan University, since 2021. He has coauthored a number of publications at dc-dc converters design and dc-ac inverters at grid connected applications. He is a Graduate Student Member with the Institute of Electrical Engineers of Japan (IEEJ). He reviewed many articles at the IEEE TRANSACTIONS ON INDUSTRIAL ELECTRONICS, IEEE TRANSACTIONS ON POWER ELECTRONICS, IEEE JOURNAL OF EMERGING AND SELECTED TOPICS IN POWER ELECTRONICS, and *IET Power Electronics*.

**MOKHTAR ALY** (Senior Member, IEEE) received the B.Sc. and M.Sc. degrees in electrical engineering from Aswan University, Aswan, Egypt, in 2007, and 2012, respectively, and the Ph.D. degree from the Department of Electrical Engineering, Faculty of Information Science and Electrical Engineering, Kyushu University, Japan, in 2017.

In 2008, he joined the Department of Electrical Engineering, Aswan University, as an Assistant Lecturer, where he has been an Assistant Professor with the Faculty of Engineering, since 2017. He worked as a Postdoctoral Researcher with the Solar Energy Research Center (SERC-Chile), Universidad Técnica Federico Santa María, Chile, from March 2019 to June 2021. He has been an Academic Researcher with Universidad San Sebastián, Santiago, Chile, since July 2021. His current research interests include reliability of power electronics systems, especially in renewable energy applications, multi-level inverters, fault tolerant control, electric vehicles, and light emitting diode (LED) lamp drivers. He is a member with the IEEE Power Electronics Society (PELS), the IEEE Industrial Electronics Society (IES), and the IEEE Power and Energy Society (PES).

**WALEED ALHOSAINI** (Member, IEEE) was born in Dawmat Aljandal, Saudi Arabia. He received the B.S. degree in electrical engineering from Jouf University, Sakaka, Aljouf, Saudi Arabia, in 2011, and the M.S. and Ph.D. degrees in electrical engineering from the University of Arkansas, Fayetteville, AR, USA, in 2015 and 2020, respectively. He is currently an Assistant Professor with the Department of Electrical Engineering, Jouf University. He also serves as the Director of the Engineering and Applied Sciences Research Unit, Jouf University. His current research interests include renewable energy systems, grid-connected systems, stand-alone systems, multilevel converters, and model predictive control. He is a member of the Eta Kappa Nu.

**EMAD A. MOHAMED** received the B.Sc. and M.Sc. degrees in electrical power engineering from Aswan University, Aswan, Egypt, in 2005 and 2013, respectively, and the Ph.D. degree in electrical power engineering from Kyushu Institute of Technology, Japan, in 2019.

He was a Demonstrator with the Department of Electrical Engineering, Aswan Faculty of Engineering, Aswan University, from November 2007 to August 2013, and an Assistant Lecturer, from 2013 to 2015. He was a Research Student with Kyushu University, Japan, from April 2015 to October 2015. He has been an Assistant Professor, since May 2019. He was in a Master Mobility Scholarship at the Faculté des Sciences et Technologies, Université de Lorraine, France. The scholarship sponsored by FFEEBB Erasmus Mundus. His current research interests include applications of superconducting power devices, power system stability, and reliability and protection.